The Journal of Experimental Biology 200, 2723–2745 (1997)
Printed in Great Britain © The Company of Biologists Limited 1997
JEB0994

THE MECHANICS OF FLIGHT IN THE HAWKMOTH *MANDUCA SEXTA*

II. AERODYNAMIC CONSEQUENCES OF KINEMATIC AND MORPHOLOGICAL VARIATION

ALEXANDER P. WILLMOTT* AND CHARLES P. ELLINGTON
Department of Zoology, University of Cambridge, Downing Street, Cambridge CB2 3EJ, UK

Accepted 4 August 1997

Summary

Mean lift coefficients have been calculated for hawkmoth flight at a range of speeds in order to investigate the aerodynamic significance of the kinematic variation which accompanies changes in forward velocity. The coefficients exceed the maximum steady-state value of 0.71 at all except the very fastest speeds, peaking at 2.0 or greater between 1 and 2 m s^{-1}. Unsteady high-lift mechanisms are therefore most important during hovering and slow forward flight. In combination with the wingtip paths relative to the surrounding air, the calculated mean lift coefficients illustrate how the relative contributions of the two halfstrokes to the force balance change with increasing forward speed. Angle of incidence data for fast forward flight suggest that the sense of the circulation is not reversed between the down- and upstrokes, indicating a flight mode qualitatively different from that proposed for lower-speed flight in the hawkmoth and other insects. The mid-downstroke angle of incidence is constant at 30–40 ° across the speed range. The relationship between power requirements and flight speed is explored; above 5 m s^{-1}, further increases in forward velocity are likely to be constrained by available mechanical power, although problems with thrust generation and flight stability may also be involved.

Hawkmoth wing and body morphology, and the differences between males and females, are evaluated in aerodynamic terms. Steady-state force measurements show that the hawkmoth body is amongst the most streamlined for any insect.

Key words: aerodynamics, hawkmoth, *Manduca sexta*, lift coefficient, power requirements, morphology.

Introduction

A detailed analysis of free flight in the hawkmoth *Manduca sexta* L. has revealed the kinematic changes as speed increases from hovering to fast forward flight (Willmott and Ellington, 1997). In this study, we investigate the aerodynamic significance of the observed kinematic variation, the power requirements for flight at different speeds and the nature of the constraints on maximum flight speed.

Insect flapping flight represents an unusual aerodynamic problem because of the inherent ‘unsteadiness’ and the low Reynolds number of the airflow. A large number of models for unsteady animal flight have been formulated, and these have been categorized and evaluated in recent reviews by Spedding (1992), Spedding and DeLaurier (1996) and Smith *et al.* (1996). The techniques range from those incorporating momentum and blade-element theories to those employing lifting-line or lifting-surface methods, but each requires non-trivial simplifying assumptions. Recent unsteady panel methods, for example, are more advanced than their predecessors in considering trailing wake vorticity and dynamic effects (Smith *et al.* 1996), and interactions between wing deformation and the aerodynamic forces (Smith, 1996), but they still have important shortcomings. In particular, they do not yet incorporate the leading-edge vortices that have a profound influence on the flow around hawkmoth wings at all speeds (Willmott *et al.* 1997) and which are likely to play a major role in insect flight aerodynamics (Ellington *et al.* 1996). At the low Reynolds numbers and high angles of incidence characteristic of insect flight, viscous effects in the near field are better addressed by Navier–Stokes solvers, which are now beginning to be applied to animal locomotion (e.g. Liu *et al.* 1996).

Advanced numerical techniques will, undoubtedly, become standard in animal flight investigations. Their introduction will, however, be delayed by the paucity of detailed and relevant empirical data for their validation and by the need to investigate fully the inherent errors in the new techniques and their applicability to other conditions (Visbal, 1986; Spedding, 1992). Accurate and reliable modelling of instantaneous forces

*Present address: Kawachi Millibioflight Project, Japan Science and Technology Corporation (JST), Park Building 3F, 4-7-6 Komaba, Meguro-ku, Tokyo 153, Japan (e-mail: sandy@kawachi.jst.go.jp).

is not an option available at present. Instead, in this report, we concentrate in more general terms on the lift-generating requirements placed on the wings during flight at different speeds and, in particular, on the possible aerodynamic consequences of the kinematic trends described in Willmott and Ellington (1997).

The 'mean coefficients' method used here is a slightly modified momentum jet/blade-element approach of the type used by Dudley (1990), Dudley and Ellington (1990*b*), Cooper (1993) and Wakeling and Ellington (1997*b*). This technique has the advantage of being the most accessible of the current models – using data on the core kinematic parameters – and of being easily modified to incorporate new kinematics or wing morphology. Despite its simplifying assumptions, the mean coefficients model has been shown in a wide range of studies (e.g. Osborne, 1951; Dudley and Ellington, 1990*b*; Dudley, 1995) to be capable of producing meaningful estimates of aerodynamic forces and power requirements. It has also generated workable hypotheses linking flight kinematics and aerodynamics, thus meeting Spedding's (1992) definition of a 'useful' aerodynamic model. Such models are necessarily refined as and when new techniques become available.

The model is used here to determine the mean lift coefficient at each of the flight speeds in the kinematic study and to estimate the associated aerodynamic and inertial power components. The coefficients are calculated under the assumption that they are constant throughout each halfstroke of the wingbeat. They thus represent the lowest possible lift coefficient required from the wings for a given set of wingbeat kinematics; if the coefficients are not constant (a more realistic scenario), then instantaneous values at certain points of the wingbeat cycle must exceed these mean values (Ellington, 1984*a*). A number of related questions are also addressed, such as the aerodynamic function of the upstroke and the aerodynamic and energetic significance of the asymmetric wingbeat. For comparative purposes, the lifting performance of hawkmoth wings and bodies under 'steady' flow conditions was measured. Finally, the morphology of adult *Manduca sexta* was investigated and the possible aerodynamic significance of the observed differences between the sexes, and between hawkmoths and other insects, is discussed.

Materials and methods

Measurement of steady-state wing and body forces

Steady-state lift and drag were measured using the optoelectronic force transducer described by Dudley and Ellington (1990*b*). A summary of its design and operation will be given here; details can be found in the earlier paper. The transducer measured the displacement in two orthogonal directions of a stainless-steel tube to which a test object was attached *via* a mounting pin. The voltage output of the transducer had a linear relationship to the moment applied to the tube, and this was calibrated at the beginning and end of each set of measurements. A range of replaceable spring elements covered forces on the test object of up to 0.016 N. The transducer was positioned at the mouth of the open-jet wind tunnel used in the kinematic study (Willmott and Ellington, 1997).

Aerodynamic forces on the body

The wings were removed from freshly killed *Manduca sexta* whose body posture was similar to that seen in free flight. Owing to the problems of orienting the legs and antennae in a realistic position, and to the difficulty in determining such positions from the high-speed videos, these structures were also removed. The body was mounted at the top of a stainless-steel entomological pin which passed through the left and right wingbases. The bodies were left to 'set' for 1 day before use in order to fix the abdomen in flight position.

Lift and drag measurements were made on six bodies for airspeeds from 1 to 5 $m\,s^{-1}$, and at the following angles of attack: −15°, 0°, 15°, 25°, 35°, 45° and 60°. The 0° angle was set with the longitudinal axis of the body parallel to the airflow; positive angles of attack refer to the body being pitched head-up with respect to the horizontal. In order to standardize the Reynolds numbers based on body length Re_b for the different bodies, the slight differences in body length were corrected for by slight modifications in the airspeed. The Reynolds numbers used were 3150, 6040, 9150, 12 270 and 15 220, corresponding to speeds of approximately 1, 2, 3, 4 and 5 $m\,s^{-1}$, respectively.

Aerodynamic forces on the wings

Before the wings were removed from the bodies of freshly killed moths, the left wing couple was moved into a realistic flight orientation. A small quantity of cyanoacrylate gel was applied between the dorsal surface of the hindwing and the ventral surface of the forewing, close to the wingbase, to hold the wings in the correct alignment. The wing couple was then detached carefully from the body by cutting through the wingbases as close as possible to the body. At this point, the anojugal flap folded under the hindwing. It was not possible to return this region to its correct position in fresh wings, and so the flap was removed by cutting along its fold line. The wing was mounted on a stainless-steel pin with the longitudinal axis of the wing aligned with the shaft of the pin: the head of the pin was removed and its final 5 mm bent perpendicular to the main shaft to form a short hook which was then attached, using a small drop of beeswax, near to the base of the underside of the wings.

The *Manduca sexta* wing is not a planar surface: a spanwise gradient of wing twist is inherent in its structure. The wing was mounted so that the chosen angle of attack corresponded to the inclination of the wing halfway between the wingbase and wingtip, close to the radius of the first moment of wing area which is where the steady-state aerodynamic force is assumed to act. The angle of attack in the proximal area of the wing was up to approximately 5° more positive than this value, whilst the angle in the distal region was up to 5° more negative. Lift and drag measurements were made at 10° angle of attack intervals from −50° to +70°, and at Reynolds numbers based on mean

wing chord Re_c of 1150, 3300 and 5560, which corresponded to airspeeds of approximately 1, 3 and 5 m s^{-1}. The measurements at Re_c=1150 were made on the day that the wings were removed. The remaining data were collected the following day.

Relative velocity and angles of incidence

The instantaneous relative velocity U_r at any given spanwise location on the wing was determined from the resultant of the forward flight velocity V, the induced velocity w_0, and the flapping velocity U at that point. The forward and flapping velocities were obtained from the free-flight kinematic data given in Willmott and Ellington (1997). The induced velocity was estimated using momentum jet theory under the assumptions that it was constant along the wingspan and over the course of the wingbeat, and that the actuator disc was approximately horizontal. The induced velocity under these conditions is vertical, and its magnitude w_0 at the actuator disc is given by the expression derived by Stepniewski and Keys (1984) for helicopters in forward flight:

$$w_0 = \sqrt{\frac{-V^2}{2} + \sqrt{k^4 w_{0,\mathrm{RF}}^4 + \frac{V^4}{4}}}, \qquad (1)$$

where $w_{0,\mathrm{RF}}$ is the Rankine–Froude estimate for the hovering induced velocity:

$$w_{0,\mathrm{RF}} = \sqrt{\frac{mg}{2\rho\Phi R^2}}, \qquad (2)$$

where m is body mass, $\boldsymbol{g}$ is gravitational acceleration, ρ is the mass density of air, Φ is stroke amplitude and R is wing length. The factor k in equation 1 corrects for temporal and spatial variation in the wake; the value of 1.2 for k suggested by Pennycuick (1975) for forward flight also corresponds well with estimates from vortex theory for hovering insect flight (Ellington, 1984*d*).

Fourier series approximations were fitted to the raw data for the positional angles. The functions for sweep angle ϕ and elevation angle θ (for definitions, see Willmott and Ellington, 1997) could be differentiated to obtain the components of the flapping velocity in the stroke plane and normal to the stroke plane, respectively. The series were truncated after the terms for the fourth harmonic because this resulted in a good, smoothed approximation to the raw data without introducing unrealistic high-order harmonics which led to excessive angular accelerations.

The body was assumed to experience the same induced velocity as the wings. The relative velocity for the body $U_{r,b}$ was calculated as the vector sum of the forward velocity V and the induced velocity w_0. The magnitude of the relative velocity was used to derive the Reynolds number for the body Re_b:

$$Re_b = \frac{U_{r,b} l}{\nu}, \qquad (3)$$

where the characteristic length l was the body length, and ν was the kinematic viscosity of air (1.55×10^{-5} m^2 s^{-1} at 23 °C).

The relative velocity of the wings was resolved into its components in three directions: tangential to the flapping velocity and parallel to the stroke plane, normal to this tangent and the longitudinal axis, and parallel to the longitudinal axis of the wing. The angle between the relative velocity and the stroke plane was determined from the first two components, and these angles were used to convert the geometric angles of rotation relative to the stroke plane α_{sp} from the kinematics study (Willmott and Ellington, 1997) into the more aerodynamically relevant angles of incidence α_r. Positive values of this parameter, which is the angle between the wing chord and the relative velocity, indicate that the air was striking the ventral surface of the wing. These angles also represent the effective angles of incidence α_r' since the zero lift angle of the wings is approximately 0 ° (see below).

The angle between the relative velocity of the body and horizontal was subtracted from the body angle χ to give the angle of incidence $\chi_{r,b}$ for calculation of the aerodynamic forces on the body.

Aerodynamic forces and mean lift requirements

The most recent and detailed version of the mean coefficients method developed by Osborne (1951) is the model developed by C. P. Ellington and successfully applied to both horizontal and vertical flight in bumblebees (Cooper, 1993). An outline only of the approach will be presented here. The application of the model to hawkmoth flight differs from those in previous studies only in the rejection, based on the kinematic analysis (Willmott and Ellington, 1997), of the assumption that the wingbeat is sinusoidal and confined to the stroke plane. The asymmetry in the wingbeat was incorporated using the Fourier series described above. The inclusion of elevation angles necessitated changes to the expressions for the components, with respect to three mutually orthogonal directions in a gravitational coordinate system, of the relative velocity U_r and of the normal to the relative velocity U_n. These modifications are described in detail in Willmott (1995).

Reconstruction of wing shape

The wing was divided into 50 strips of equal spanwise width using a beta function to model the distribution of area in the wing planforms obtained in Willmott and Ellington (1997). Matching this function to the measured first and second moments of wing area results in a close approximation of *Manduca sexta* wing shape (Ellington, 1984*b*) and gives an analytical function which is readily incorporated into the aerodynamic model. The root mean square difference between the real and predicted chord widths for the three moths was 3.3 %.

Wing forces

At any given time in the wingbeat cycle, the instantaneous lift force L and drag force D acting on an individual wing strip are given by:

$$L = \frac{1}{2}\rho c\,dr\,U_r^2 C_L, \qquad (4)$$

$$D = \frac{1}{2}\rho c\,dr\,U_r^2 C_{D,\mathrm{pro}}, \qquad (5)$$

where U_r and c are the relative velocity and chord of the strip,

respectively, dr is the spanwise width of the strip, C_L is the lift coefficient, $C_{D,pro}$ is the profile drag coefficient, and ρ is the density of air (1.19 kg m^{-3} at 23 °C). The component of U_r parallel to the wing axis is ignored. C_L and $C_{D,pro}$ are unknown at this point, but are assumed to be constant throughout a halfstroke. The sign of C_L during the upstroke depends upon whether the oncoming air is striking the ventral surface (C_L is positive) or the dorsal surface (C_L is negative) of the wing.

The lift and drag forces for each strip were resolved into their vertical and horizontal components, and these components were then summed along the wingspan and over the period of each halfstroke. The vertical forces (in the z direction) resulting from the lift and drag forces, respectively, during the downstroke (subscript d) were calculated using the following expressions:

$$L_{z,d} = A_{z,d}C_L, \qquad D_{z,d} = B_{z,d}C_{D,pro}, \tag{6}$$

where

$$A_{z,d} = \frac{1}{2}\rho dr\sum_t\sum_i c\left(U_{n,z}\right)^2, \tag{7}$$

$$B_{z,d} = \frac{1}{2}\rho dr\sum_t\sum_i c\left(U_{r,z}\right)^2, \tag{8}$$

with the double summations being taken over the strip number (i, from 1 to 50) and time (t) in the downstroke. $U_{r,z}$ and $U_{n,z}$ are the vertical components of the relative velocity and of the normal to the relative velocity, respectively, for strip i at time t. The downstroke horizontal forces ($A_{x,d}$, $B_{x,d}$), and the upstroke forces ($A_{x,u}$, $B_{x,u}$, $A_{z,u}$, $B_{z,u}$), were determined in an analogous manner.

The horizontal and vertical forces can be balanced to give a set of simultaneous equations for the two mean force coefficients $\overline{C}_L$ and $\overline{C}_{D,pro}$ which are:

$$F_z = \overline{C}_L(A_{z,d} \pm A_{z,u}) + \overline{C}_{D,pro}(B_{z,d} + B_{z,u}), \tag{9}$$

$$F_x = \overline{C}_L(A_{x,d} \pm A_{x,u}) + \overline{C}_{D,pro}(B_{x,d} + B_{x,u}), \tag{10}$$

where the selected sign for $A_{z,u}$ and $A_{x,u}$ corresponds to the assumed sign of the upstroke lift coefficient. F_z is the vertical force required to balance the weight $m\boldsymbol{g}$ minus any vertical components of body lift and drag, and F_x is the horizontal force required to overcome the parasite drag. The values of F_z and F_x are known, and the mean coefficients can, in theory, be found by solving equations 9 and 10. In practice, the horizontal forces are small relative to the vertical forces, even at high forward speeds, and the coefficients are very sensitive to errors in the horizontal components (Dudley and Ellington, 1990*b*). If the purpose of the modelling is to estimate mean lift coefficients, then a more pragmatic approach is to assign a realistic value to the mean drag coefficient and then to solve for the mean lift coefficient using equation 9.

Determining a precise value for the drag coefficient is difficult, but the lift coefficient is relatively insensitive to its value (Dudley and Ellington, 1990*b*). For each flight sequence, the mean lift coefficient was calculated using two different estimates of the mean profile drag coefficient. The first was Ellington's (1984*e*) approximation for insect wings operating at relatively high angles of incidence and at a Reynolds number Re_c of a few thousand or lower,

$$C_{D,pro} \approx \frac{7}{\sqrt{Re_c}}. \tag{11}$$

At the somewhat higher Reynolds numbers typical of *Manduca sexta* flight, this relationship gives values of approximately 0.1, which are markedly lower than the measured steady-state drag coefficients for angles of incidence appropriate to flight (see below). The latter include induced drag as well as profile drag, but it is still likely that equation 11 underestimates the profile drag coefficient for *Manduca sexta*. An attempt was made, therefore, to obtain a second, more realistic estimate for $C_{D,pro}$ using data on the angles of incidence and the steady-state drag coefficients. The angles of incidence for the inner and outer wing sections at the mid-point of each halfstroke were determined, where possible, from the angles of rotation and the inclination of the relative velocity. The mean for the two sections was taken as the representative angle for each halfstroke, and the profile drag coefficient for this angle, interpolated from the steady-state values and corrected for the contribution from induced drag (Willmott, 1995), was used as the mean coefficient for the halfstroke. The two halfstrokes were treated separately because the upstroke angles of incidence were consistently lower than those during the downstroke. The choice of profile drag coefficient had little impact on the mean lift requirement, but it has more significant implications for the profile power requirements.

A mean estimate for Re_c, the Reynolds number based on the wing chord, was obtained by averaging the instantaneous Reynolds number for individual strips along the wingspan and over the course of the wingbeat.

Aerodynamic forces on the body

The aerodynamic forces on the body were calculated using the relative velocity of the body $U_{r,b}$ and the angle of incidence $\chi_{r,b}$ determined above. The coefficients for the forces parallel and normal to the relative velocity, at the appropriate Reynolds numbers and angles of incidence, were found by interpolation from the measured steady-state values. The resultant force at each speed was resolved into vertical and horizontal components, which correspond to the parasite lift L_{par} and parasite drag D_{par}, respectively. In order to investigate the significance of the estimates of induced velocity on the body forces, the parasite lift and drag were also calculated using only the forward velocity.

Calculation of mechanical power requirements

Induced power

The induced power P_{ind} was calculated using the expression:

$$P_{ind} = w_0(m\boldsymbol{g} - B_z C_{D,pro}), \quad (12)$$

where B_z is the sum of $B_{z,d}$ and $B_{z,u}$. This is a departure from previous models, where the induced power was simply $w_0 m\boldsymbol{g}$ (but see also Wakeling and Ellington, 1997*b*). The modification recognises that the vertical component of profile drag cannot be ignored when considering the energetic cost of generating weight support. Three potential cases exist under which induced power must be calculated: for no net vertical component of profile drag, for a net upward force, and for a net downward force. Equation 12 is common to all three.

In the first case, when $B_z C_{D,pro}$ is zero, the momentum jet must generate a vertical force equal to the entire weight of the insect, $m\boldsymbol{g}$. The induced power associated with the jet is the product of the thrust and the appropriate induced velocity w_0, calculated from equations 1 and 2. This special case is equivalent to the model used in earlier studies. When $B_z C_{D,pro}$ is positive, however, profile drag contributes to weight support, and the thrust requirement for the momentum jet is reduced accordingly. A new, lower induced velocity should be calculated by replacing $m\boldsymbol{g}$ in equation 2 with the reduced value for thrust, and the thrust and induced velocity iterated until the induced power converges. This would be a time-consuming process for what would only be a second-order correction to P_{ind}. The first-order correction given by equation 12 is pragmatic wherever the contribution of profile drag to the vertical force balance is small. The validity of this assumption will be discussed below.

In the final case, profile drag contributes a net downwards vertical component, $B_z C_{D,pro}$ is negative, and the momentum jet thrust must be increased for net weight support. From equation 12, the induced power also increases. The total power requirement for weight support is higher here than in the first two cases (in which the total is identical). The additional power produces no extra useful aerodynamic force. Instead, it represents energy wasted by the conflicting flows of the net upwash created by air dragged along with the wings and the downwash from the momentum jet.

Profile power

The instantaneous profile power P_{pro} required to overcome the profile drag is the summation along the wing of the products of sectional profile drag and relative velocity. The total profile power over the wingbeat is calculated from a similar summation to that used for profile drag:

$$P_{pro} = \tfrac{1}{2}\rho \mathrm{d}r\, C_{D,pro} \sum_t \sum_i c U_r^3. \quad (1$$

Parasite power

The parasite power P_{par} required to overcome parasite drag is given by the product of the parasite drag and the forward flight speed:

$$P_{par} = V D_{par}. \quad (14)$$

Inertial power

Inertial power P_{acc} is required to accelerate the wings early in each halfstroke. The mean value over the wingbeat is the sum of the kinetic energy imparted to the wings during the up- and downstrokes divided by the cycle period:

$$P_{acc} = nI\left[\left(\frac{\mathrm{d}\omega}{\mathrm{d}t}\right)^2_{max,u} + \left(\frac{\mathrm{d}\omega}{\mathrm{d}t}\right)^2_{max,d}\right], \quad (15)$$

where n is the wingbeat frequency, ω is the radian frequency and I is the moment of inertia of the wings and their virtual mass. The values in parentheses are the maximum angular velocities during the upstroke and downstroke, respectively, resulting from changes in both sweep and elevation angle:

$$\frac{\mathrm{d}\omega}{\mathrm{d}t} = \sqrt{\left(\frac{\mathrm{d}\phi}{\mathrm{d}t}\right)^2 + \left(\frac{\mathrm{d}\theta}{\mathrm{d}t}\right)^2}. \quad (16)$$

Equation 15 gives the mean value for inertial power over the two halfstrokes. In the asymmetric *Manduca sexta* wingbeat, the mean inertial power during the longer downstroke acceleration will be lower than this, while the mean inertial power during the upstroke will be higher.

During the deceleration phase of each halfstroke, kinetic energy is released by the wing. This energy can be used for aerodynamic work, and any excess may either be stored as elastic energy or dissipated as heat and sound (Ellington, 1984*e*).

Total mechanical power required from the flight muscle

The aerodynamic power P_{aero} is the sum of the induced, parasite and profile powers. The mean total mechanical power required from the flight muscles over the course of the wingbeat must include the fourth component, the inertial power. If the metabolic cost of doing negative work during wing deceleration is assumed to be negligible compared with the cost of doing positive work, then the mean positive mechanical power depends upon the extent to which any excess negative work during deceleration can be stored in elastic structures in the thorax/flight muscle system. Ellington (1984*e*) derived expressions for the total mean positive mechanical power requirements P_{pos} for hovering flight under the two extreme conditions of perfect and zero elastic storage. For forward flight, parasite power must be added to Ellington's (1984*e*) equations which, using the terminology adopted in the present paper, then become:

$$P_{pos} = P_{aero} \quad (17)$$

for perfect elastic storage, and

$$P_{pos} = \frac{1}{2}\left(P_{aero} + P_{acc}\right) \quad (18)$$

for zero elastic storage.

The mechanical power requirements and their components were all normalized to body-mass- and muscle-mass-specific values, to facilitate comparison of the values among the different moths, and between *Manduca sexta* and other species.

Wing and body morphology

A range of morphological parameters were measured for six

male and seven female moths (including the three moths from the kinematic study; Willmott and Ellington, 1997). These parameters are defined in the Symbols list, and the methods used to determine them were those described by Ellington (1984*a*), with the exception of the radii of wing mass which were found by the strip-cutting approach he used for smaller insects rather than the compound pendulum technique. The wing area (and associated virtual mass) parameters were measured from the video images obtained in Willmott and Ellington (1997), with each wing divided into 50 strips of equal spanwise width.

Results

Steady-state aerodynamic characteristics of the body and wings

The mean lift and drag coefficients for the *Manduca sexta* bodies are presented as a polar diagram in Fig. 1. The coefficients were calculated using the planform area of the bodies, and each point is the mean of measurements from six moths. Standard error bars for the means are not shown since most were smaller than the symbol size: the mean standard errors for the drag and lift coefficients were 0.018 and 0.021, respectively. The plotted lines show how the coefficients change with angle of attack at a constant Reynolds number Re_b: the curves are very similar as far as an angle of attack of 35 °, but at the highest angles they diverge slightly with both lift and drag coefficients increasing with Reynolds number.

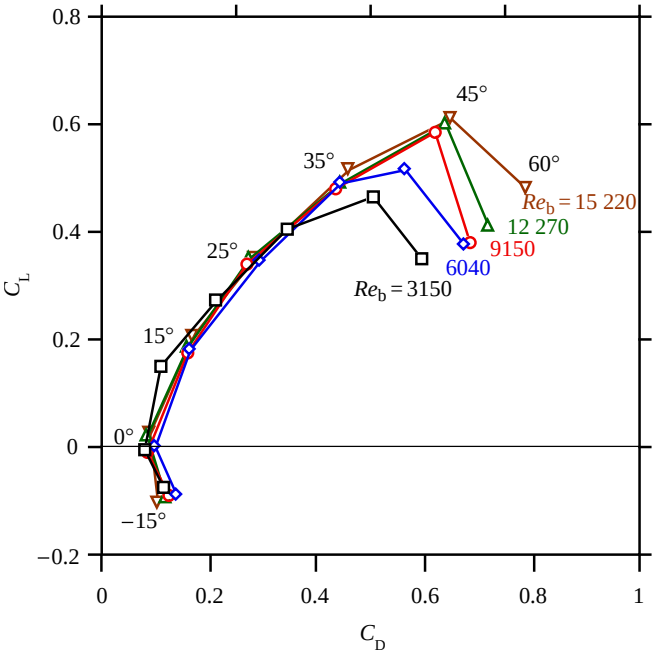

Fig. 1. Polar diagram showing the aerodynamic characteristics of *Manduca sexta* bodies. Each point is the mean from six bodies. The different curves represent the force coefficients at five different Reynolds numbers Re_b, which are given at the right of the figure. The angle of attack, in degrees, is shown close to each cluster of points. C_L, lift coefficient; C_D, drag coefficient.

The lift coefficients for the body increased steadily with increasing angle of attack from close to zero at 0 ° to a maximum of 0.6 at 45 ° and the highest Reynolds numbers, before decreasing to approximately 0.4 at 60 °. The drag coefficients increased steadily with increasing inclination from a minimum of 0.08 at 0 ° to reach 0.78 at 60 ° and Re_b=15 220. The mean lift force under the maximum lift conditions (45 ° and Re_b=15 220) was 22.4 % of body weight, but the body angles observed during free flight at 5 m s^{-1} were in the region of 15 and 25 °, and the relative body lift at these angles averaged 7.4 and 12.8 %, respectively. The maximum drag force, at 60 ° and Re_b=15 220, was 29.5 % of body weight, but this dropped to 6.3 and 10.3 % at 15 and 25 °, respectively.

The maximum lift:drag ratio is a measure of the aerodynamic performance of the body. For *Manduca sexta* bodies, this ratio ranged from 1.18 at Re_b=6040 to 1.38 at Re_b=3150. The latter value was recorded at an angle of attack of 15 °, but the maximum slope at every other Reynolds number occurred at an angle of 25 °.

The mean force coefficients, based on wing planform area, for the wing couples are presented as a polar diagram in Fig. 2. The three curves represent the changes with angle of attack at Reynolds numbers Re_c (using the mean chord as the characteristic length) of 1150, 3300 and 5560. The mean standard errors were 0.03 for the lift coefficients and 0.02 for the drag coefficients. The general C-shaped forms of the curves are similar, but at positive angles of attack, the coefficients, especially the lift coefficient, were lower at Re_c=1150 than at the two higher speeds.

The minimum drag coefficients at each speed, ranging from 0.05 at Re_c=5560 to 0.07 at Re_c=1150, were recorded at an angle of attack of 0 °. The zero-lift angle of attack was 0 ° at the lowest speed, but it was at a small negative angle (approximately −2 to −3 °) at the higher speeds. The lift coefficients increased sharply between 0 and 10 °, with only a slight increase in drag coefficient, before levelling off to a plateau from 20 to 40 ° of approximately 0.7 at Re_c=5560, 0.65 at Re_c=3300, but only 0.45 at Re_c=1150. The maximum lift coefficients at these Reynolds numbers were 0.71 (at 20 °), 0.67 (at 30 °) and 0.46 (at 40 °), respectively. The lift coefficients decreased steadily at angles of attack greater than 40 °, falling to between 0.24 and 0.34 at 70 °. The drag coefficients increased almost linearly with angle of attack from 10 to 70 °. At angles of attack of 20 ° or more, the direction of the resultant of the lift and drag forces on the wing was always within 2 ° of the normal to the wing chord.

The wing performance at negative angles of attack was similar at all three Reynolds numbers and approximated the reflection in the line C_L=0 of the curve for positive angles at Re_c=1150. The most negative value for lift coefficient was −0.43 at Re_c=1150 and an angle of attack of −40 °. At the highest two Reynolds numbers, the lift and drag coefficients were smaller in magnitude than those at the corresponding positive angle of attack.

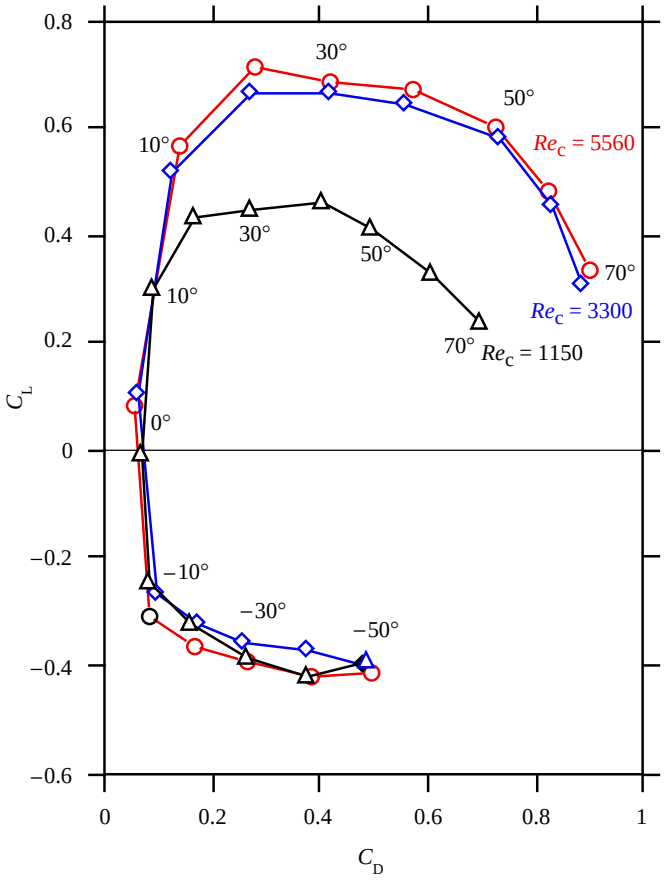

Fig. 2. Polar diagram for the aerodynamic characteristics of *Manduca sexta* wings. Each point is the mean from four wing couples. The different curves correspond to measurements at three different Reynolds numbers Re_c, which are shown at the right of the figure. The angles of attack, in degrees, are indicated at intervals along the length of the curves. C_L, lift coefficient; C_D, drag coefficient.

The wings were most aerodynamically efficient, indicated by the maximum lift:drag ratio, at 10 ° for all three airspeeds. The C_L:C_D ratios were 3.4 at Re_c=1150, 4.2 at Re_c=3300 and 4.0 at Re_c=5560.

Relative velocities and wingtip paths

The forward and induced velocities are given in Table 1, along with the mean flapping velocity at the wingtip $\bar{U}_t$ (=2Φ*nR*), the reduced frequency parameters, and the Reynolds numbers for the body and wings. The induced velocity was largest, both in absolute terms and relative to the forward and flapping velocities, at the lower flight speeds. It exceeded the forward velocity at speeds below 2 m s^{-1}, but then declined steadily in importance as flight speed increased. The mean wingtip flapping velocity was more constant because of the low variation in the wingbeat frequency and stroke amplitude. The high amplitude during hovering flight led to a flapping velocity over 5 m s^{-1}, but at all faster speeds the flapping velocity fell within the range 4.2–5 m s^{-1}.

The comparative uniformity of the mean flapping velocity resulted in the advance ratio J (=$V/\bar{U}_t$) rising linearly with forward velocity, from approximately 0.2 at 1 m s^{-1} to 1.1 at 5 m s^{-1}. The reduced frequency parameter k (=ω$\bar{c}$/2V) correspondingly fell from 1.5 to 0.3 over the same speed range. The Reynolds numbers for the wings and the body (Re_c and Re_b, respectively) both tended to increase with flight speed as a result of increases in the appropriate relative velocity; the only exception was a decrease for the wing between 0 and 1 m s^{-1} as the lower flapping and induced velocities more than offset the increase in forward velocity. All of the wing Reynolds numbers Re_c at speeds below 5 m s^{-1} fell between the values for the steady-state measurements at 3 and 5 m s^{-1}.

The wingtip paths relative to the surrounding air for moth F2 are shown in side view in Fig. 3A; the paths for the other moths were very similar. Each curve corresponds to the motion during three successive wingbeats at one of the six different flight speeds. The path starts at the lower left, with the wings at the supination position. The subsequent wing motion follows the path in the direction of the arrow; the relative velocity experienced by the wing is in the opposite direction.

The axis of the wingtip path during hovering flight is vertical owing to the absence of any forward component in the relative velocity. The motion during the translatory periods of each halfstroke is inclined at only a small angle to the horizontal; the upstroke path doubles back over the preceding downstroke. As the forward speed increases, the overall axis of the motion becomes less inclined and there is increasing asymmetry between the two halfstrokes, both in terms of their length and their orientation. The direction of the downstroke motion is remarkably constant across the speed range, but its length increases steadily with forward speed. The upstroke, in contrast, varies in direction rather than length, with its inclination becoming less retrograde with increasing forward speed. When the latter reaches 5 m s^{-1}, it is sufficiently large relative to the flapping velocity that the wingtip moves forward relative to the surrounding air during both halfstrokes.

Angles of incidence of the wings

The orientation of the wing chord relative to the oncoming air in the middle of each halfstroke is shown in Fig. 3B. The curves show the wing path at 0.5*R* for moth F2 at flight speeds of 0, 0.9, 2.9 and 5 m s^{-1}. Wing chords, with the short perpendicular arm indicating the ventral side of the leading edge, have been drawn to scale at the middle of most halfstrokes; the arrowheads immediately upstream of the chords signify the direction of the relative velocity at these points. No data were available for the wing inclination during the upstroke at 2.9 m s^{-1}. The angle of incidence for each chord is the average over both the outer and inner wing sections. Details of the individual angles of incidence are shown in Table 2, along with the original angles of rotation (see Willmott and Ellington, 1997) and the $C_{D,pro}$ estimates, which were derived from the mean angles of incidence for use in the aerodynamic force analysis.

The angles of incidence in the mid-downstroke were all positive, indicating that the air was striking the ventral surface of the wing. At most speeds, air hits the dorsal surface during

Table 1. *The induced velocity* w_0, *mean wingtip velocity* $\bar{U}_t$, *advance ratio* J, *reduced frequency parameter* k *and Reynolds numbers for the wings and body (*Re_c *and* Re_b, *respectively) at each flight velocity V*

Moth	V ($m\,s^{-1}$)	w_0 ($m\,s^{-1}$)	$\bar{U}_t$ ($m\,s^{-1}$)	J	k	Re_c	Re_b
M1	0	1.42	5.06	0	–	4222	3874
	1.0	1.38	4.55	0.22	1.47	3898	4596
	2.0	0.96	4.77	0.42	0.74	4744	5970
	2.9	0.74	4.49	0.65	0.53	4587	8221
	3.9	0.59	4.30	0.91	0.37	5325	10699
F1	0	1.30	5.78	0	–	4752	3523
	1.1	1.21	5.05	0.22	1.36	4137	4428
	3.0	0.65	4.80	0.63	0.48	4699	8340
	4.0	0.50	4.18	0.96	0.33	5315	10956
	5.0	0.41	4.48	1.12	0.29	5919	13635
F2	0	1.47	5.23	0	–	4913	4041
	0.9	1.41	4.91	0.18	1.69	4377	4579
	2.1	1.07	4.49	0.47	0.70	4370	6473
	2.9	0.86	4.61	0.63	0.53	5072	8319
	3.8	0.64	4.63	0.82	0.39	5435	10599
	5.0	0.48	4.72	1.06	0.30	6559	13819

See the text and Symbols list for a full description of the parameters.

the upstroke, resulting in negative angles of incidence. At $5\,m\,s^{-1}$, however, the upstroke angle for moth F2 became positive; the forward inclination of the upstroke caused air to strike the ventral surface during both halfstrokes. The absence of wing orientation data at 2.9 and $3.8\,m\,s^{-1}$ prevents identification of the speed at which the transition from negative

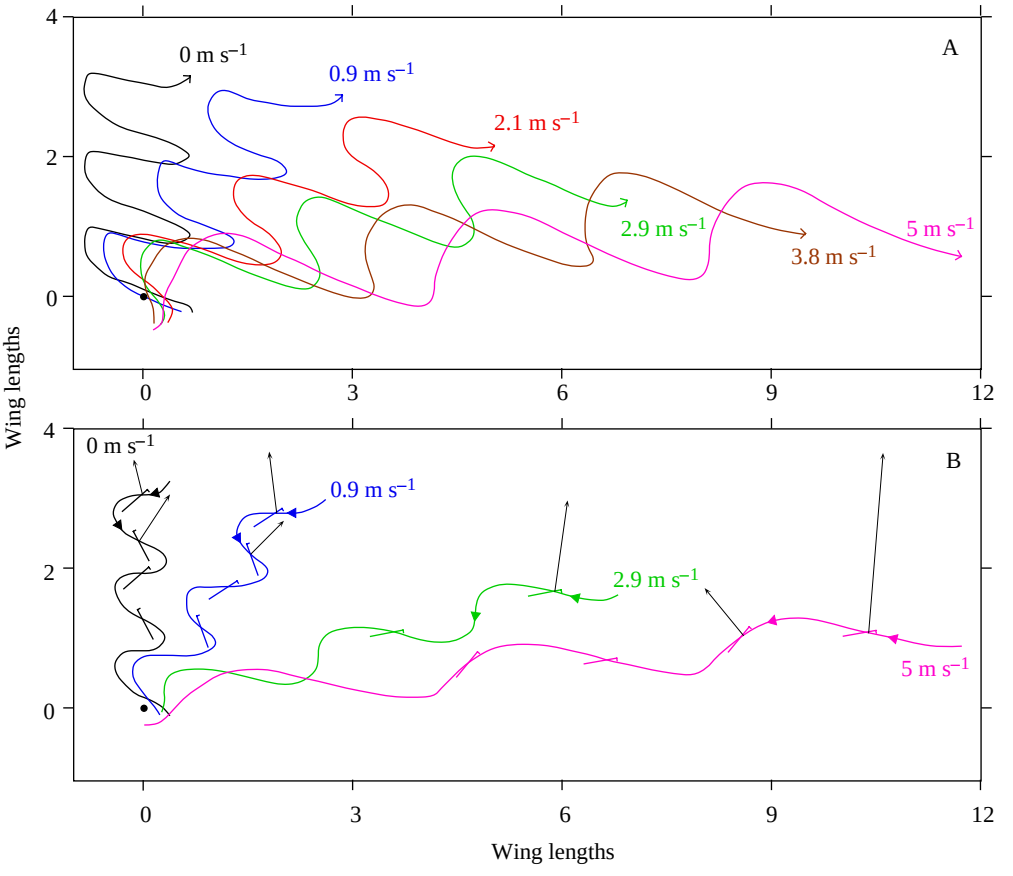

Fig. 3. The wing paths relative to the surrounding air for moth F2, seen in side view. (A) The path at the wingtip for each of the six flight speeds; arrows indicate the direction of motion of the path. (B) The path at 0.5*R* for four of these speeds, where *R* is wing length. The mean orientation of the wing chords is shown in the middle of most halfstrokes along with an estimate of the direction and relative magnitude of the resultant halfstroke force at that speed (black arrows). Upstroke data at $2.9\,m\,s^{-1}$ were not available. The initial position of the wingbase is indicated by the filled black circle, and the units are wing lengths. The arrowheads on the wing paths in B indicate the direction of the relative velocity at these points. See the text for further explanation.

to positive angles of incidence occurs. This speed almost certainly varies with spanwise position. Comparison of the wing paths for 0.5*R* (Fig. 3B) and 1.0*R* (Fig. 3A) demonstrates that the magnitude and direction of the relative velocity change substantially along the length of the wing. The upstroke path is directed forward in the middle of the wing at speeds as low as 2.9 m s^{-1}, whereas it does not have this direction at the wingtip until 5 m s^{-1}.

There was no clear trend with increasing speed for the downstroke angle of incidence, although there was a tendency for the angle to be lower at the higher speeds (Fig. 4). Comparing the angles of rotation α_{sp} and incidence α_r, correcting for the orientation of the local velocity reduces both the absolute values for the angle of incidence and the discrepancy in angle between the inner and outer wing sections (Fig. 4). Above 2 m s^{-1}, the angle of incidence was almost constant along the length of the wing. The vast majority of the mid-downstroke angles of incidence were between 20 and 40 °, matching the plateau region on the wing lift polar in Fig. 2. The mid-upstroke angles were lower than the downstroke values at all speeds for which the former could be determined (Table 2).

A combination of the trends in wing paths and the angles of incidence with increasing forward speed leads to marked changes in the resultant forces for the two halfstrokes. First approximations of the relative magnitudes and directions of these forces at 0.5*R*, as estimated from the wing paths and the calculated mean lift and drag coefficients (see below), are shown in Fig. 3B.

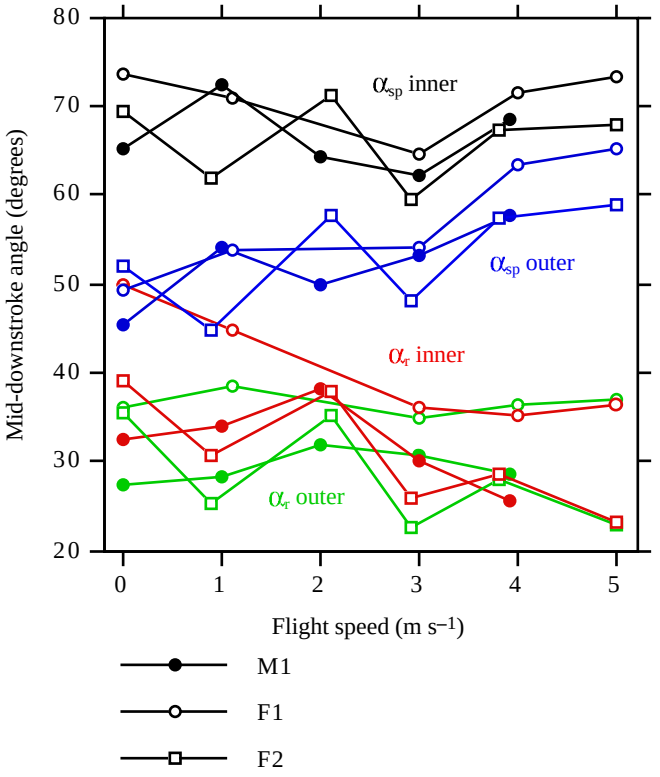

Fig. 4. A comparison of the trends with increasing flight speed in mid-downstroke angle of rotation α_{sp} and angle of incidence α_r. Data are presented separately for each moth, and for the inner and outer functional wing sections. The trends are described further in the text.

Body angles and forces

The estimated angles of incidence for the bodies, and the associated aerodynamic forces, are given in Table 3. At hovering and low forward velocities, the relative velocity was dominated by the induced velocity and thus was closer to vertical than horizontal. This can be seen in the conversion of large positive body angles into large negative angles of incidence. At the higher flight speeds, the induced velocities were lower and their effect was merely to keep the angle of incidence slightly lower than the measured body angle. The angles of incidence were typically approximately 10 ° or less at speeds above 2 m s^{-1}, with the notable exception of the 24 ° angle for moth F1 at 5 m s^{-1} which resulted from its unusually high body angle.

The interpolated body lift and drag coefficients (Table 3) were used to estimate the steady-state parasite lift $\hat{L}_{par}$ and parasite drag $\hat{D}_{par}$, expressed as percentages of the body weight. With the exception of moth F1 at 5 m s^{-1} (where both forces exceeded 12 %), all of the parasite forces were less than 6 % of body weight. At low speeds, the negative sign for the estimated angles of incidence resulted in a negative vertical force and some thrust, but their contributions to the force balance were negligible. A comparison of the parasite lift and drag forces with those calculated only from the forward velocity demonstrated that the inclusion of induced velocity resulted in a small reduction in body lift and parasite drag. With the exception of F1 at 5 m s^{-1} (where the discrepancies in $\hat{L}_{par}$ and $\hat{D}_{par}$ were 3.8 and 2.1 %, respectively), the differences were less than 2.7 % of body weight for parasite lift and less than 1.3 % for parasite drag. The reduction in the forces was most marked at high forward velocities, where the direction of the relative velocity reduced the body angles (the geometric angles of attack) to effective angles of incidence of less than 10 °. The body forces estimated from the relative velocity were used in the calculations of parasite power and the mean lift coefficients for the wings.

Mean lift coefficients

The mean wing lift coefficient $\bar{C}_L$ required to balance the vertical forces in each flight sequence was determined for each of four cases, the differences between which relate to the nature of the assumed upstroke aerodynamics and to the shape of the function used to describe the flapping motion. Using the true asymmetric wingbeat described by the Fourier series approximations, the mean lift coefficient was calculated for reversed upstroke circulation (the air striking the morphological dorsal surface), for an inactive upstroke, and for the air striking the ventral surface during the upstroke. In order to investigate the aerodynamic significance of the asymmetry between the two halfstrokes, the mean lift coefficients were also determined for a sinusoidal wingbeat with the same wingbeat amplitude and mean sweep angle. The mean profile

Table 2. *The angles of rotation α_{sp} and angles of incidence α_r for the inner (I) and outer (O) wing sections at mid-downstroke and mid-upstroke*

		Mid-downstroke						Mid-upstroke					
	V	α_{sp} (degrees)		α_r (degrees)				α_{sp} (degrees)		α_r (degrees)			
Moth	($m\,s^{-1}$)	I	O	I	O	Mean	$C_{D,pro}$	I	O	I	O	Mean	$C_{D,pro}$
M1	0	65.2	45.5	32.4	27.4	29.9	0.28	129.4	150.1	–28.4	–17.0	–22.7	0.14
	1.0	72.5	54.2	34.0	28.4	31.2	0.30	137.7	154.0	–20.0	–17.8	–18.9	0.11
	2.0	64.4	50.0	38.3	31.9	35.1	0.35	–	145.7	–	–20.8	–	–
	2.9	62.1	53.1	30.2	30.8	30.5	0.29	120.1	145.2	–11.3	–15.6	–13.5	0.08
	3.9	68.4	57.8	25.7	28.7	27.2	0.23	–	–	–	–	–	–
F1	0	73.7	49.2	49.9	36.1	43.0	0.50	139.8	159.3	–20.9	–15.8	–18.4	0.11
	1.1	71.0	53.9	44.8	38.6	41.7	0.48	116.6	141.7	–33.2	–21.0	–27.1	0.20
	3.0	64.5	54.2	36.1	35.0	35.6	0.36	–	132.8	–	–17.4	–	–
	4.0	71.5	63.5	35.3	36.3	35.8	0.36	–	–	–	–	–	–
	5.0	73.2	65.2	36.5	37.0	36.8	0.37	–	–	–	–	–	–
F2	0	69.5	52.0	39.2	35.5	37.4	0.39	129.0	148.7	–38.6	–27.2	–32.9	0.22
	0.9	61.8	44.7	30.6	25.3	27.9	0.25	126.4	150.1	–27.9	–21.1	–24.5	0.15
	2.1	71.2	57.8	37.9	35.3	36.6	0.38	122.0	142.4	–21.8	–28.0	–24.9	0.15
	2.9	59.6	48.1	25.9	22.6	24.3	0.20	–	–	–	–	–	–
	3.8	67.4	57.3	28.5	27.9	28.2	0.25	–	–	–	–	–	–
	5.0	67.8	59.0	23.1	23.0	23.1	0.17	118.4	118.9	26.1	3.0	14.6	0.10

The missing mid-upstroke values indicate cases in which the rotation angles could not reliably be determined from the digitized frames (see Willmott and Ellington, 1997).

The mean angles of incidence were used to estimate the profile drag coefficient $C_{D,pro}$.

See text for full details.

V, flight velocity.

Table 3. *The relative velocity $U_{r,b}$ and angle of incidence $\chi_{r,b}$ of the body for each flight sequence, along with the estimated body force coefficients and the parasite lift $\hat{L}_{par}$ and drag $\hat{D}_{par}$ forces (as percentages of body weight)*

Moth	V ($m\,s^{-1}$)	$U_{r,b}$ ($m\,s^{-1}$)	χ (degrees)	$\chi_{r,b}$ (degrees)	C_L	C_D	$\hat{L}_{par}$ (%)	$\hat{D}_{par}$ (%)
M1	0	1.4	40.0	–50.0	–0.48	0.61	–1.90	–1.51
	1.0	1.7	29.4	–26.0	–0.36	0.30	–1.97	–0.56
	2.0	2.2	21.0	–5.2	–0.04	0.12	–0.65	0.70
	2.9	3.0	17.4	3.1	0.05	0.11	0.23	1.70
	3.9	3.9	14.4	5.7	0.09	0.13	1.62	3.28
F1	0	1.3	35.1	–54.9	–0.43	0.64	–1.61	–1.08
	1.1	1.6	26.5	–21.0	–0.28	0.22	–1.40	–0.21
	3.0	3.1	25.8	13.6	0.18	0.17	1.92	2.84
	4.0	4.0	15.7	8.6	0.12	0.14	2.45	3.77
	5.0	5.0	28.7	24.0	0.37	0.30	12.93	12.28
F2	0	1.5	34.6	–55.4	–0.44	0.65	–1.79	–1.20
	0.9	1.7	28.4	–28.9	–0.40	0.34	–1.78	–0.54
	2.1	2.4	26.7	–0.1	–0.00	0.11	–0.35	0.68
	2.9	3.0	21.1	4.6	0.06	0.12	0.30	1.56
	3.8	3.9	19.5	10.0	0.14	0.15	2.07	3.20
	5.0	5.0	16.3	10.8	0.16	0.16	4.71	5.65

V, flight velocity; χ, geometric body angle; C_L, lift coefficient; C_D, drag coefficient.

See text for full details.

drag coefficients $\bar{C}_{D,pro}$ were calculated from the Reynolds number for the wings, using equation 11. Replacing the mean profile drag coefficients by the values based on the observed angles of incidence (which were up to five times larger) had little impact on the mean lift coefficient; the difference between the two estimates was never greater than 0.08.

The changes with forward speed in the lift coefficient requirements, and the significance of the wingbeat shape and upstroke mode can be seen in Fig. 5. For each of the moths, the variation in mean lift coefficient is shown for the asymmetric wingbeat, for the sinusoidal approximation, and for the asymmetric wingbeat under the assumption of an inactive upstroke. For the former two cases, the required lift coefficient was calculated under both the assumption of a negative and a positive upstroke lift coefficient, but only the lower of the two values is plotted. Open symbols indicate that the lower value resulted from the assumption of a negative upstroke lift coefficient (i.e. a reversed upstroke circulation), and filled symbols that the assumed upstroke coefficient was positive (i.e. for air striking the ventral wing surface during the upstroke as well as the downstroke). A reversed lift coefficient, indicating a negative upstroke angle of incidence, was advantageous at low speeds, but positive angles of incidence throughout the beat resulted in lower required lift coefficients at the highest speeds. The transition for each moth occurred at the speed where $A_{z,u}$ changed from negative to positive: for the asymmetric wingbeat this was at $4\,m\,s^{-1}$, for the sinusoidal motion it was at $3\,m\,s^{-1}$.

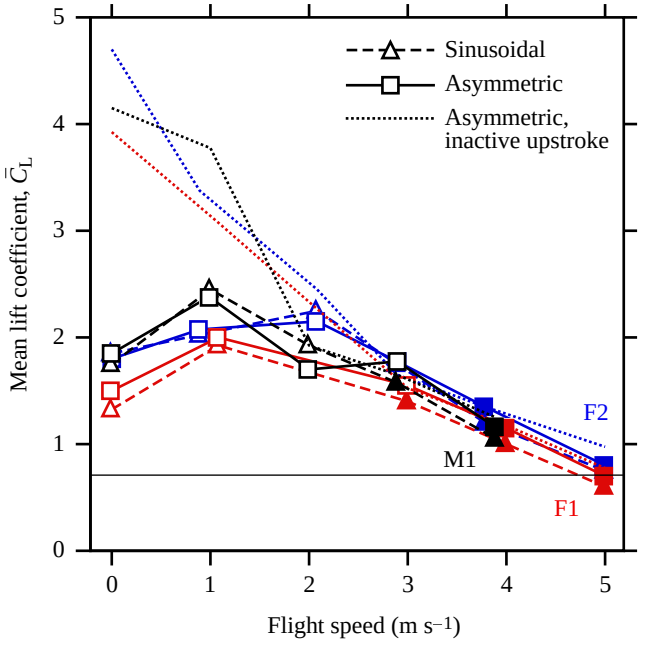

Fig. 5. The mean lift coefficients $\bar{C}_L$ calculated for three different combinations of assumed upstroke function and wingbeat shape. Data are given for the true, asymmetric wingbeat (squares), for the sinusoidal approximation to the wingbeat (triangles) and for the asymmetric wingbeat under the assumption of an aerodynamically inactive upstroke (no symbols). The first two cases include both a reversed and a non-reversed upstroke circulation; only the lower of the two calculated coefficients is shown. Open symbols indicate that the reversed upstroke circulation resulted in the lower lift requirement, filled symbols that the non-reversed circulation was preferable. The data for the individual moths are distinguished by colour. The horizontal line at 0.71 indicates the maximum lift coefficient obtained from a *Manduca sexta* wing couple under steady-state conditions.

An initial increase in mean lift coefficient from hovering to a maximum at $1–2\,m\,s^{-1}$ was characteristic of all the curves assuming an active upstroke. The maximum values for the true, asymmetric wing motion ranged from 1.98 for F1 to 2.38 for M1. Lift coefficient declined steadily with further increases in flight speed, falling to minimum values at $5\,m\,s^{-1}$ of 0.70 and 0.80 for F1 and F2, respectively. These compare with the maximum steady-state value of 0.71 which is indicated by the horizontal line in Fig. 5. The calculated mean lift coefficients for the sinusoidal motion were comparable to, but usually slightly lower than, those for the asymmetric wingbeat; the minimum values for moths F1 and F2 were 0.59 and 0.75 at $5\,m\,s^{-1}$. The relative magnitudes of the coefficients for the asymmetric and sinusoidal wingbeats depended upon which upstroke angle of incidence option was assumed. With negative angles, the lift coefficients still decreased with forward speed, but more slowly, and the sinusoidal estimates were higher than the asymmetric wingbeat values.

Aerodynamic contributions of the two halfstrokes

Qualitative changes in the relative contributions of the two halfstrokes to thrust and weight support were shown in Fig. 3B. The arrows originating at the aerodynamic centre of each wing chord represent the direction and magnitude of the resultant force vector from each halfstroke, as estimated from the length and direction of the halfstroke paths and the calculated mean force coefficients. Both halfstrokes provided weight support during hovering, but the upstroke was more important. By $2.9\,m\,s^{-1}$, however, weight support was largely restricted to the downstroke, but with the upstroke still capable of providing significant thrust if the angle of incidence was negative. At $5\,m\,s^{-1}$, the downstroke generated substantial weight support and some thrust under both upstroke assumptions, but the magnitude of the forces depended greatly upon the sign of the upstroke lift coefficient. If this was negative, then the upstroke produced thrust but negative weight support, which had to be offset by larger vertical forces during the subsequent downstroke. The mean lift coefficient, and thus the vertical force required from the downstroke, was lower if the upstroke coefficient was positive (as shown in Fig. 3B), but there was little if any net thrust under these conditions.

Mechanical power requirements

The body-mass-specific aerodynamic and inertial power components for each flight sequence are summarized in Table 4. Aerodynamic power was calculated for three of the cases considered in the mean lift coefficient analysis: for the real, asymmetric wingbeats with mean profile drag coefficients estimated from equation 11, for sinusoidal motion with the

Table 4. *Body-mass-specific power components for each flight sequence*

Moth	V ($m\,s^{-1}$)	P^*_{par} ($W\,kg^{-1}$)	P^*_{pro} ($W\,kg^{-1}$)	$P^*_{pro,s}$ ($W\,kg^{-1}$)	$P^*_{pro,ai}$ ($W\,kg^{-1}$)	P^*_{ind} ($W\,kg^{-1}$)	$P^*_{ind,s}$ ($W\,kg^{-1}$)	$P^*_{ind,ai}$ ($W\,kg^{-1}$)	P^*_{aero} ($W\,kg^{-1}$)	$P^*_{aero,s}$ ($W\,kg^{-1}$)	$P^*_{aero,ai}$ ($W\,kg^{-1}$)	P^*_{acc} ($W\,kg^{-1}$)	$P^*_{acc,s}$ ($W\,kg^{-1}$)
M1	0	0.00	3.24	3.32	5.47	14.48	14.46	14.82	17.72	17.78	20.29	27.41	27.53
	1.0	0.00	2.67	2.49	4.54	14.21	14.13	14.40	16.87	16.62	18.94	20.29	18.97
	2.0	0.13	4.34	3.64	–	9.82	9.76	–	14.29	13.54	–	43.13	23.86
	2.9	0.48	4.00	4.72	8.91	7.53	7.54	7.33	12.02	12.74	16.72	20.30	23.47
	3.9	1.24	5.78	6.20	–	6.05	6.02	–	13.07	13.47	–	24.34	18.25
F1	0	0.00	4.52	4.68	9.39	13.36	13.27	13.67	17.88	17.96	23.06	38.47	37.38
	1.1	0.00	3.16	3.47	9.43	12.36	12.29	12.88	15.53	15.76	22.31	21.55	26.25
	3.0	0.84	4.38	5.13	–	6.52	6.55	–	11.74	12.52	–	20.28	23.16
	4.0	1.48	5.97	6.72	–	5.08	5.10	–	12.54	13.30	–	26.19	17.27
	5.0	6.02	7.74	10.26	–	4.14	4.24	–	17.91	20.53	–	17.94	20.80
F2	0	0.00	3.82	3.29	9.98	15.07	15.01	16.00	18.89	18.30	25.98	29.57	23.04
	0.9	0.00	2.86	3.00	5.29	14.37	14.30	14.74	17.23	17.31	20.04	18.52	20.34
	2.1	0.14	2.85	3.09	7.96	10.87	10.80	11.21	13.86	14.03	19.30	14.60	16.05
	2.9	0.44	4.16	4.10	–	8.70	8.70	–	13.30	13.24	–	20.70	17.44
	3.8	1.19	4.92	5.69	–	6.50	6.47	–	12.61	13.36	–	16.50	16.69
	5.0	2.77	7.91	9.05	13.96	4.92	4.93	4.88	15.60	16.74	21.60	15.87	17.62

Body-mass-specific profile P^*_{pro}, induced P^*_{ind} and total aerodynamic P^*_{aero} power are given for three cases: for the asymmetric wingbeat (no subscript), for the sinusoidal wing motion (subscript 's') and for the asymmetric wingbeat with profile drag estimated from the observed angles of incidence (subscript 'ai').

The body-mass-specific parasite power P^*_{par} is common to all three cases.

P^*_{acc}, body-mass-specific inertial power.

See the text for full details.

V, flight velocity.

same drag coefficients, and for the asymmetrical kinematics but using the individual upstroke and downstroke profile drag coefficients estimated from the angles of incidence. The subscripts 's' and 'ai' denote the second and third cases, respectively. The power requirements are independent of the sign of the upstroke lift coefficient. The values for parasite power were common to all three cases, but there were differences in the induced and profile powers and, therefore, in the total aerodynamic power. The inertial power required during wing acceleration is given for both the asymmetric and sinusoidal kinematics.

The trends in power with increasing forward speed were qualitatively similar for all three cases, and are illustrated in Fig. 6 for moth F2 and the first case. The solid lines describe the trends in aerodynamic power and its three components for the asymmetric wingbeat using the lower estimates of mean profile drag. The dark blue crosses show the markedly increased profile power when the higher profile drag coefficients were used in the model. Estimates for aerodynamic power and its components at $6\,m\,s^{-1}$ are also presented; they will be used below as evidence for possible power constraints on maximum flight speed. The estimates were calculated by extrapolation from the kinematic parameters at speeds up to $5\,m\,s^{-1}$. The wing motion within the stroke plane was assumed to be the same as at $5\,m\,s^{-1}$, but modified values of 63.5° and 13.6° were assigned to the stroke plane and body angles, respectively. Wingbeat frequency was taken to be 25 Hz.

For moths M1 and F2, the aerodynamic power was highest during hovering, with the induced power contributing substantially more than half of the total power requirement (Table 4). Induced power decreased slightly between hovering and $1\,m\,s^{-1}$, and thereafter more rapidly with increasing flight speed. Above $2\,m\,s^{-1}$, this decrease was partially offset by the increases in parasite and profile power, but the total requirement did not reach its minimum until 3 or $4\,m\,s^{-1}$. At higher speeds, the profile and parasite powers increased more steeply, and the total aerodynamic power rose again.

The magnitude of the aerodynamic power requirement was dependent upon the value assigned to the profile drag coefficient. For the profile drag coefficients of approximately 0.1, derived from equation 11, the aerodynamic power decreased from 17–19 $W\,kg^{-1}$ at hovering to a minimum of 12–13 $W\,kg^{-1}$, before increasing to over 15 $W\,kg^{-1}$ at $5\,m\,s^{-1}$. The markedly higher profile drag coefficients used in the third case resulted in correspondingly higher profile power requirements, raising the aerodynamic power to values between 17 and 26 $W\,kg^{-1}$.

The net vertical contribution from profile drag was always in the opposite direction to weight support, resulting in induced power estimates at all flight speeds which were greater than the value of $w_0 m\boldsymbol{g}$ which would have been obtained using the simpler model from previous studies. The increase in induced power ranged from 3 to 5% for the lower profile drag coefficients, and up to 11% for the higher coefficients. For the

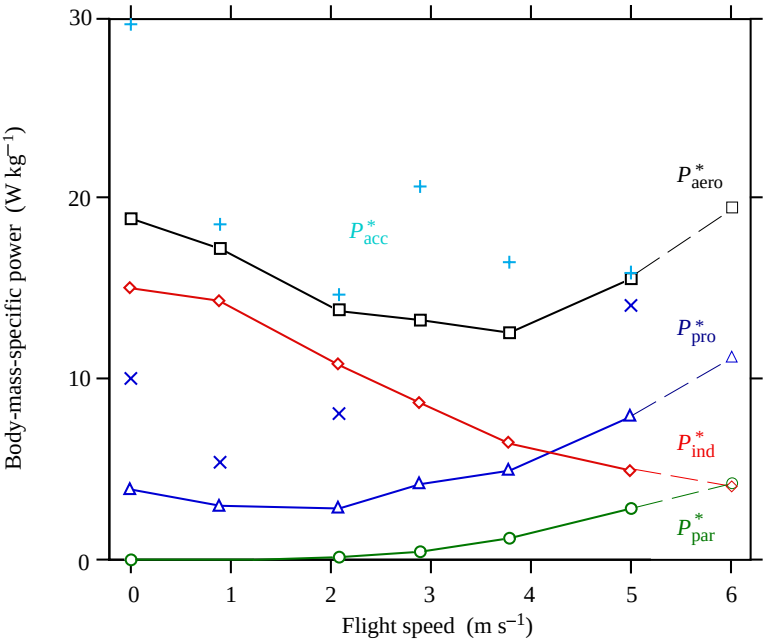

Fig. 6. The variation in total body-mass-specific aerodynamic power P^*_{aero} and its components with forward speed for moth F2. The dark blue crosses are the body-mass-specific profile power P^*_{pro} when the profile drag coefficients are estimated from the observed angles of incidence; the corresponding profile power values using the lower profile drag coefficients derived from equation 11 are shown by the open triangles and the dark blue curve. Body-mass-specific inertial power estimates P^*_{acc} (pale blue crosses), assuming zero elastic storage and a sinusoidal wingbeat, are given for comparison with the magnitude of the aerodynamic power. The kinematic values used to calculate the power components at 6 m s^{-1} were extrapolated from the data for lower speeds. See the text for full details. P^*_{ind}, body-mass-specific induced power; P^*_{par}, body-mass-specific parasite power.

lower coefficients, the associated increase in total aerodynamic power decreased from 4 % at hovering to 1 % at 5 m s^{-1}.

The inertial power estimates are also given in Table 4 and Fig. 6, for comparison with the magnitude of the aerodynamic power. The cost of accelerating the wings was at least as high as the total aerodynamic requirements, and often much greater, especially at low speeds. The inertial power for the asymmetric wingbeats was very susceptible to the large variations in flapping velocities that arose from differentiation of the Fourier series for the positional angles. The estimates were as high as 43 W kg^{-1}. The values calculated for the sinusoidal motion are more robust functions of the stroke amplitude and wingbeat frequency, and they probably represent a more reliable estimate of the power that must be transferred to the accelerating wings. These values for inertial power were, therefore, used in the estimation of total positive mechanical power.

Body-mass-specific and muscle-mass-specific estimates for the mean positive mechanical power requirements are shown in Table 5. The body-mass-specific values for perfect elastic storage are the same as for the aerodynamic powers P^*_{aero} and $P^*_{aero,ai}$ in Table 4. The muscle-mass-specific total positive power requirements correct for the variation in the proportion of body mass which is flight muscle: 22.8, 19.7 and 16.2 %, respectively, for moths M1, F1 and F2. For moth F2 at three speeds, the aerodynamic power using the higher profile drag coefficients was larger than the inertial power. In this situation, the net work during deceleration remains positive, and so the extent of elastic storage need not be considered. The positive mechanical power requirements for zero elastic storage, shown in parentheses, are therefore assumed to be the same as the values for perfect elastic storage.

If zero elastic storage is assumed, the power estimates increase by 24 % on average. Increases of up to approximately 50 % were observed for moths M1 and F1, whose wing masses were higher relative to body mass than that of F2; the largest increase for F2 was only 16 %. Inertial power was highest for hovering flight, where the stroke amplitudes were largest; during forward flight, the inertial cost was approximately constant (Fig. 6). The general shape of the curve of mechanical power against flight speed, and thus the minimum power speed, was therefore relatively independent of the assumed extent of elastic storage. The higher profile drag coefficients led to an average increase of 29 % in the mean total positive mechanical power.

Wing and body morphology

The values of the body parameters for the three moths used in the kinematic study (Willmott and Ellington, 1997), and mean values for a total of six male and seven female moths (including those used in the kinematic study), are presented in Table 6. The results of *t*-tests for the difference between the means for the males and females show that the latter were significantly heavier than the males, and that a greater proportion of their mass was located in the abdomen, leading to a relatively more posterior location for the centre of gravity. Surprisingly, the shift in the centre of gravity did not change the free body angle χ_0. The body length relative to the wing length, $\hat{L}$, was more than 10 % lower in the female moths than in the males.

Wing parameter data are also given in Table 6. Data for only four males are presented; the wings of the remaining two males were too worn to be included. The wings of the females were significantly longer, but relatively narrower, than those of the males. The higher aspect ratio of the females, in conjunction with their greater body weight, resulted in a higher wing

Table 5. *Body-mass-specific and muscle-mass-specific estimates for mean total positive mechanical power* P^*_{pos}

		Body-mass-specific power		Muscle-mass-specific power			
		Zero storage		Zero storage		Perfect storage	
Moth	V (m s^{-1})	P^*_{pos} (W kg^{-1})	$P^*_{pos,ai}$ (W kg^{-1})	P^*_{pos} (W kg^{-1})	$P^*_{pos,ai}$ (W kg^{-1})	P^*_{pos} (W kg^{-1})	$P^*_{pos,ai}$ (W kg^{-1})
M1	0	22.63	23.91	99.24	104.86	77.73	88.98
	1.0	17.92	18.96	78.61	83.15	74.00	83.08
	2.0	19.07	–	83.66	–	62.67	–
	2.9	17.75	20.10	77.83	88.14	52.71	73.33
	3.9	15.66	–	68.68	–	57.30	–
F1	0	27.63	30.22	140.23	153.38	90.74	117.03
	1.1	20.89	24.28	106.04	123.24	78.83	113.23
	3.0	17.45	–	88.58	–	59.61	–
	4.0	14.90	–	75.65	–	63.64	–
	5.0	19.35	–	98.24	–	90.89	–
F2	0	20.97	(25.98)	129.43	(160.38)	116.62	160.38
	0.9	18.78	20.19	115.95	124.62	106.36	123.70
	2.1	14.96	(19.30)	92.33	(119.15)	85.57	119.15
	2.9	15.37	–	94.88	–	82.11	–
	3.8	14.65	–	90.41	–	77.81	–
	5.0	16.61	(21.60)	102.55	(133.35)	96.32	133.35

Values are given for the cases of zero and perfect elastic storage, and for profile drag coefficients estimated from equation 11 (no additional subscript) and from the observed angles of incidence (subscript 'ai').

Values in parentheses indicate wingbeats in which the net work during wing deceleration is positive; thus, P^*_{pos} under the assumption of zero elastic storage is the same as for perfect storage.

See text for full details.

V, flight velocity.

loading p_w but a lower wing mass $\hat{m}_w$ relative to body mass. The shape parameters representing the distribution of wing area and mass were not significantly different in the two sexes. There were significant differences in the radii of the first two moments of virtual mass, $\hat{r}_1(v)$ and $\hat{r}_2(v)$, but the discrepancies between the means were less than 1 % of wing length.

Discussion

The mean lift coefficients analysis of the kinematic data has provided a number of useful insights into the aerodynamics of hawkmoth flight. The most important finding is that the lift coefficient required to balance the vertical forces exceeded the maximum steady-state value of 0.71 at all speeds below 5 m s^{-1}, indicating that additional unsteady, high-lift aerodynamic mechanisms must be operating. Even at 5 m s^{-1}, the correspondence between the maximum steady-state coefficients and the *mean* requirement cannot be taken as proof that steady-state mechanisms are sufficient for providing weight support (Ellington, 1984*a*). The advance ratios did not significantly exceed 1, even at the highest speeds, so a dependence on unsteady mechanisms at all flight speeds would be expected (Spedding, 1992). Similar conclusions have been reached for the flight of bumblebees (Dudley and Ellington, 1990*b*; Cooper, 1993) and flies (Dudley, 1987; Ennos, 1989).

Higher advance ratios, however, are associated with the low wingbeat frequencies recorded for other lepidopterans (Betts and Wootton, 1988; Dudley and DeVries, 1990; Dudley, 1990; Bunker, 1993), and it is possible that their fast forward flight may be less reliant on unsteady mechanisms. Using a mean lift coefficient of 1.0 as the maximum consistent with steady aerodynamics, Dudley and DeVries (1990) found that the flight of the moth *Urania fulgens* at speeds above 2 m s^{-1}, and advance ratios over 1, could be explained without invoking high-lift mechanisms. For the hawkmoth, however, wake visualization showed that a leading-edge vortex was a major component of a highly three-dimensional flow at all flight speeds, and that it actually grew in size as the speed increased (Willmott *et al.* 1997). The weight of evidence from experimental and numerical studies suggests that unsteady, high-lift mechanisms make a significant contribution to flight at all except possibly the very highest advance ratios.

It is equally clear that the magnitude of the unsteady contribution, as indicated by the discrepancy between the mean lift coefficient and the maximum steady-state value, varies with forward speed. For *Manduca sexta*, the maximum mean lift coefficient was at 1–2 m s^{-1}. The required mean lift coefficient at hovering was slightly lower, and the coefficients also decreased steadily at speeds greater than 2 m s^{-1}. A peak in mean lift coefficient at a low, but non-zero, flight speed has

Table 6. *Body and wing morphology for the moths in the kinematic study (Willmott and Ellington, 1997), and means for larger samples of male and female* Manduca sexta

	M1	F1	F2	Male mean ± S.E.M.	Female mean ± S.E.M.	*t*-test significance
Body parameters				(*N*=6)	(*N*=7)	
m (mg)	1579	1648	1995	1199±110	1833±112	**
$\hat{L}$	0.876	0.811	0.817	0.965±0.025	0.852±0.012	**
$\hat{l}$	0.489	0.530	0.540	0.467±0.015	0.529±0.007	**
$\hat{l}_1$	0.256	0.311	0.287	0.221±0.010	0.291±0.004	***
$\hat{l}_2$	0.344	0.401	0.358	0.337±0.008	0.369±0.006	**
χ_o	82.9	82.8	76.3	79.6±1.0	79.2±1.1	
$\hat{m}_t$	28.4	25.0	17.8	33.0±2.3	21.1±0.9	***
$\hat{m}_{tm}$	22.8	19.7	16.2	27.0±1.6	17.7±0.5	***
$\hat{m}_a$	54.1	57.8	61.6	42.4±3.4	61.7±1.1	***
Wing parameters				(*N*=4)	(*N*=7)	
R (mm)	48.5	51.9	52.1	47.3±0.6	51.0±0.9	*
p_w (N m^{-2})	8.93	8.53	10.33	7.75±0.78	9.73±0.35	*
AR	5.28	5.65	5.52	5.20±0.13	5.53±0.04	*
$\hat{r}_1$ (S)	0.445	0.447	0.450	0.449±0.001	0.451±0.001	
$\hat{r}_2$ (S)	0.514	0.515	0.518	0.517±0.001	0.518±0.001	
$\hat{r}_3$ (S)	0.564	0.565	0.567	0.566±0.002	0.567±0.001	
$\hat{v}$	1.07	1.08	1.08	1.08±0.00	1.08±0.00	
$\hat{r}_1$ (v)	0.413	0.418	0.425	0.419±0.002	0.424±0.002	*
$\hat{r}_2$ (v)	0.475	0.479	0.483	0.478±0.001	0.482±0.001	**
$\int \hat{c}^3 \hat{r} \mathrm{d}\hat{r}$	0.469	0.480	0.492	0.479±0.006	0.495±0.003	*
$\int \hat{c}^{\frac{3}{2}} \hat{r}^{\frac{5}{2}} \mathrm{d}\hat{r}$	0.199	0.201	0.204	0.202±0.001	0.204±0.001	
$\hat{m}_w$ (%)	5.93	5.79	4.49	6.52±0.59	5.02±0.18	*
$\hat{h}$ (%)	0.081	0.072	0.067	0.080±0.002	0.072±0.001	**
$\hat{r}_1$ (m)	0.293	0.297	0.292	0.310±0.007	0.298±0.003	
$\hat{r}_2$ (m)	0.376	0.378	0.379	0.392±0.007	0.383±0.003	

See the Symbols list for definition of the parameters. The right-hand column shows the results of *t*-tests of the difference between the means for male and female moths.

Key to significance levels: *P<0.05; **P<0.01; ***P<0.001.

also been reported for bumblebees (Dudley and Ellington, 1990*b*; Cooper, 1993) and hoverflies (Dudley, 1987), the only other studies of individual insects over a range of speeds. The decrease in mean lift coefficient at high speeds was more marked for *Manduca sexta* than for bumblebees (Dudley and Ellington, 1990*b*; Cooper, 1993) or hoverflies (Dudley, 1987), even with a negative upstroke lift coefficient as in the earlier studies. The reduction was more dramatic still for *Manduca sexta* if the wing was assumed to be operating at positive angles of incidence during the upstroke. This change in wing orientation is beneficial only where the upstroke path, relative to the surrounding air, is directed forwards. For the most distal regions of the wing this criterion is not met until 5 m s^{-1}, but for the middle of the wing it is reached before 3 m s^{-1}.

For asynchronous species, the large flapping velocities associated with their high wingbeat frequencies mean that the upstroke path is directed backwards at all speeds (Nachtigall, 1966; Dudley and Ellington, 1990*b*). There are changes, however, in the aerodynamic functions of the two halfstrokes with increasing forward speed; as demonstrated by Ellington's (1995) analysis of the bumblebee data from Dudley and Ellington (1990*a*). As advance ratios increase, the downstroke will increasingly dominate weight support as the associated wing path becomes longer. The upstroke contributes thrust at all speeds but its contribution decreases with increasing forward speed, a trend that is offset by an increasing thrust component from the downstroke force.

The trends in the resultant forces predicted for *Manduca sexta* flight are similar, at least up to forward speeds of 3–4 m s^{-1} (advance ratios of 0.8–0.9). The transition to positive upstroke angles of incidence at higher speeds, which is suggested by the data for moth F2 at 5 m s^{-1}, is unexpected. This switch can be viewed, using the data for mean lift coefficient, as a means of reducing the lifting performance required from the wings. Such a change should be regarded as speculative at present, however, because of the paucity of data for angle of incidence, and the fact that the data are subject to errors both in the angle of rotation and in the direction of the relative velocity. If the transition in angle of incidence is genuine then, to the best of the authors' knowledge, *Manduca sexta* is the first insect species for which a non-reversed upstroke has been proposed. In other species (including *Urania*

fulgens at all speeds), the aerodynamic underside of the wing, and thus the sense of circulation, is thought to be reversed between successive halfstrokes (Brodsky and Ivanov, 1984; Dudley and DeVries, 1990; Dudley and Ellington, 1990*b*).

The possible aerodynamic functions of the upstroke have been considered more thoroughly for flying vertebrates (e.g. Rayner, 1979, 1986; Norberg, 1985, 1990; Spedding, 1992). The upstroke is aerodynamically inactive in general, as a result of wing folding, during slow forward flight in birds and bats (Spedding, 1992), although it may generate small amounts of thrust (Norberg, 1985). At intermediate speeds, however, the upstroke becomes active as the wing path changes from a backwards to a forwards direction (e.g. Norberg, 1976; Spedding, 1987). Aldridge (1986) found a gradual change in the kinematics and aerodynamics of forward flight in the greater horseshoe bat *Rhinolophus ferrumequinum*, with the upstroke changing from thrust generation at low speeds to weight support at intermediate speeds. At the highest speed, 4.8 m s^{-1} (J=0.93), the upstroke angles of incidence were large and positive, contributing weight support but also negative thrust to the force balance. The morphological limitations on wing span and area reduction placed on insects and bats mean that *Manduca sexta* is faced with the same aerodynamic options for the upstroke as *Rhinolophus ferrumequinum*: the wing may be operated at very low angles of incidence in order to minimize the aerodynamic forces, at positive angles of incidence for weight support or at negative angles for thrust production. The final option is the usual case for insects, but in *Manduca sexta* it would generate thrust at the expense of considerable negative weight support. The second case provides additional weight support, thus decreasing the required mean lift coefficient, but it also generates negative thrust. If this is the case for *Manduca sexta* at 5 m s^{-1} then, as can be seen in Fig. 3B, the insect is struggling to produce a net positive thrust.

A final observation concerning quasi-steady aerodynamic force production is that the asymmetric wingbeat does not appear to provide an aerodynamic advantage over sinusoidal motion if positive upstroke angles of incidence are an option. However, if the upstroke angles of incidence remain negative, then the mean lift coefficients for the sinusoidal wingbeat are consistently higher than those for the asymmetric wingbeat at high flight speeds. It must be noted that any benefits of the asymmetric wingbeat may not be revealed by a quasi-steady analysis, which assumes that force production is proportional to the square of relative velocity. Lift from unsteady mechanisms, such as a leading-edge vortex, may not scale with relative velocity in the same way. Without further information, no conclusions can be drawn on the aerodynamic significance of an asymmetric wingbeat. The profile power estimates (Table 4) provide some evidence that there may be a slight energetic advantage to the asymmetric wingbeat at fast forward speeds: at speeds of 4 m s^{-1} and above, the profile power for the asymmetric wingbeat was lower, but typically by less than 15 %, than the value for the corresponding sinusoidal motion.

Aerodynamic power for flight

The U-shaped relationship between forward speed and specific aerodynamic power for *Manduca sexta* is consistent with power curves drawn for a wide range of insect (reviewed in Cooper, 1993) and vertebrate (reviewed in Norberg, 1990) fliers. The precise shape does vary, from the J-shape found by Cooper (1993) for bumblebees to the deep U-shape obtained by Rayner (1979) for a range of birds, but these represent two extreme points on a continuum of shapes derived from the same basic trends in the aerodynamic power components. The increases in aerodynamic power at the two ends of the speed range result from different components (Pennycuick, 1968), and much of the variation between species is explicable and to be expected from such diverse morphologies and kinematics.

The initial decrease in flight power from hovering to the minimum power speed results from a decrease in induced power. Parasite power is negligible at these speeds, and the profile power, whilst not negligible, is fairly constant. The location of the minimum power speed depends upon how rapidly the sum of profile and parasite power increases relative to the decrease in induced power. Profile power increases as the cube of the relative velocity (equation 13), not the forward velocity as stated by Spedding (1992). This difference is considerable for animals such as bumblebees, whose flight is characterized by low advance ratios. The flapping velocity dominates the relative velocity and, where frequency and amplitude vary little with forward speed, the profile power is approximately constant over almost all the speed range, as clearly seen with bumblebee flight (Dudley and Ellington, 1990*b*; Cooper, 1993). The advance ratios for *Manduca sexta* flight increase more rapidly with forward speed, and this is reflected in the steeper curve for profile power. In contrast, the parasite power remains small and accounts for less than half of the increase in the sum of profile and parasite power. The bumblebee body is less streamlined, however, and the parasite power contributes in large part to the increase in aerodynamic power at high forward speeds (Cooper, 1993). The relative importance of parasite power is also very sensitive to the chosen body angle, as can be seen in the discrepancy between the results at high flight speeds for moth F1 and moths M1 and F2 (Table 4), and between the different curves for pigeons derived by Pennycuick (1968) and Rayner (1979), for which different body angles were assumed (Norberg, 1990).

For any species, the curve for total aerodynamic power becomes increasingly steep at high speeds. Induced power is still decreasing, but this is offset by the ever more rapid increase in the profile and parasite components.

The correction to the traditional expression for induced power (equation 12), which results from consideration of the vertical contribution from profile drag, ranged from 3 to 11 % for *Manduca sexta*, depending upon the selected profile drag coefficient. The same increase for dragonfly and damselfly flight averaged 12 % (Wakeling and Ellington, 1997*b*). The magnitude of this correction is therefore comparable to those from previous modifications to the simple momentum jet

model to incorporate temporal and spatial effects (Ellington, 1984*d*), which have been adopted as standard in subsequent studies.

A net downwards force from profile drag is probably typical of flight in most insects. If the profile drag coefficients are similar during the two halfstrokes, and the vertical components of the flapping velocities are approximately equal and opposite, then this net downwards force is a consequence of the induced velocity. Flight in which there is a net upwards force from profile drag, whilst less common, is not unknown. The generation of large vertical forces by pressure drag during the downstroke has been identified by Ellington (1980) and Sunada *et al.* (1993) for take-off flight in butterflies from the genus *Pieris*. Weight support of this kind requires a near-vertical stroke plane with high angles of incidence during the downstroke, and low angles during a 'feathered' upstroke. Similar kinematics have been reported by Betts and Wootton (1988) as one of the flight modes used during both hovering and fast forward flight in butterflies. Profile drag will have a substantial vertical component under these conditions, and second-order corrections to P_{ind} should be incorporated.

Total mechanical power requirements

Estimates of the total mechanical power required for flight can be determined by two independent methods: from data for aerodynamic and inertial power, and from the product of muscle efficiency and the metabolic cost of flight (Casey, 1981). Comparing the two estimates can shed light on the extent of elastic storage in the thorax and/or wings. Casey (1981), for example, found good agreement between a metabolic estimate for the total body-mass-specific mechanical power for *Manduca sexta* hovering (47.4 W kg^{-1}, assuming 20 % muscle efficiency) and the estimated sum of aerodynamic power (14.6 W kg^{-1}, modified from Weis-Fogh, 1973) and inertial power (36.4 W kg^{-1}). He concluded that the inertial costs of hovering flight were not significantly reduced by an elastic system in the thorax, in contrast to Weis-Fogh's (1972) finding for the closely related privet hawkmoth *Sphinx ligustri*.

Recalculating the metabolic estimate of total mechanical power from Casey's (1976) measured body-mass-specific metabolic cost of flight (237 W kg^{-1}) and the muscle efficiency of 10 % determined experimentally by Stevenson and Josephson (1990) for *Manduca sexta* dorsoventral muscle, the available body-mass-specific power is only 23.7 W kg^{-1}. The inertial power component has been greatly reduced, but not completely removed. Similarly, Wilkin and Williams (1993) concluded that elastic storage was effective at a flight speed of 3.36 m s^{-1}, but that some power was still available, if needed, to damp the wing oscillations.

The specific mechanical power requirements obtained in the present study do not provide an unequivocal conclusion about the extent of elastic storage. The highest performance during flight was most likely to have been reached in moth F2, which had both the highest wing loading and the lowest percentage of flight muscle. The total muscle-mass-specific mechanical power for this moth, assuming perfect elastic storage, reached 117 W kg^{-1} during hovering, and over 160 W kg^{-1} if the higher estimates of profile power were used. These compare with a mean specific power output of 90 W kg^{-1} of flight muscle and a maximum of 130 W kg^{-1} at muscle temperatures and cycle frequencies which corresponded well with free-flight values (Stevenson and Josephson, 1990). The inertial power estimates for *Manduca sexta* were not much higher than the aerodynamic power, however, and most of the estimates for total mechanical power with no elastic storage were also within the range observed in the earlier study. The potential for considerable elastic storage has been demonstrated indirectly by the observation that, in a *Manduca sexta* with the thoracic nervous system removed, a downstroke generated by electrical stimulation of the depressor muscle can be followed by a nearly normal, passive upstroke (S. Dierkes, personal communication). The possibility remains that the storage is far from perfect, but the percentage of elastic storage cannot be quantified accurately at present.

The capacity for elastic storage does not need to be considerable. Dickinson and Lighton (1995) found that in *Drosophila hydei*, another species in which aerodynamic power and inertial power are very similar in magnitude, the cost of flight can be minimized with an elastic storage capacity as low as 10 % of the inertial power. The remaining 90 % of the inertial energy can be usefully converted to aerodynamic work during wing deceleration. The equivalent storage capacity to minimize costs for *Manduca sexta* is approximately 30 % of the inertial power.

Limits to maximum flight speed

The discussion of the kinematics and aerodynamics of fast forward flight can be extended to consider the question of what limits the maximum speed of *Manduca sexta*. For such a large insect, the maximum observed speed is surprisingly low. The highest value recorded by Stevenson *et al.* (1995) was 5.3 m s^{-1} while their calculations, based on body size, suggested that *Manduca sexta* should be capable of speeds of at least 7–10 m s^{-1}. One potential constraint in their study and in the current one was the use of flight chambers. This will undoubtedly affect flight behaviour, as it did for a range of butterflies whose typical flight speeds during insectary studies were significantly lower than those observed in the wild (Srygley and Dudley, 1993). Other observations, however, suggest that flight chambers and their size may not be so important in determining maximum speed. Cooper (1993) obtained significantly higher flight speeds from bumblebees in a wind tunnel whose closed working area was much smaller than the largest arena (an ice rink) used by Stevenson *et al.* (1995). Given sufficient motivation for flight, chamber size may not limit flight speed. There was clearly no shortage of motivation in the moths filmed in the present study: several moths tried repeatedly to reach the feeder at 5 m s^{-1}, but they appeared to have great difficulty in flying at these very fast speeds.

The available mechanical power is often considered to be the major constraint on maximum forward speed (e.g.

Pennycuick, 1968). The muscle-mass-specific power requirement for moth F2 was 96 W kg^{-1} at 5 m s^{-1}, below the hovering level of 117 W kg^{-1}, but by 6 m s^{-1} the cost is estimated to rise to 125 W kg^{-1} (Fig. 6), close to the maximum power output recorded by Stevenson and Josephson (1990). The error associated with these estimates is not known, but they suggest that this individual (the most gravid female) was operating at close to its maximum power output during hovering and that power constraints would have prevented flight speeds much in excess of 5–6 m s^{-1}.

The higher proportion of flight muscle in the other two hawkmoths resulted in lower muscle-mass-specific power requirements which shifted the power curve vertically downwards, as they did for bumblebees (Cooper, 1993). These moths would not be constrained by power limitations until speeds of well over 6 m s^{-1}, especially if the current estimates for the maximum power available from synchronous flight muscle substantially underestimate the true value, as concluded by Dudley (1995) for asynchronous muscle.

The data for *Manduca sexta* suggest that at least two other considerations may also play a part in limiting flight speed. The first of these concerns the generation of sufficient thrust at very fast speeds where parasite drag is rising rapidly. The downstroke provides most of the thrust, but its horizontal component is not substantial. The upstroke, as mentioned above, could contribute thrust but at the expense of negative lift. The increasingly forward upstroke path would only exacerbate this problem as speed increased further. The upstroke angle of incidence data at these speeds are far from unequivocal, but it appears that the upstroke is generating weight support and negative thrust. Interestingly, *Urania fulgens* flight has been recorded at markedly higher advance ratios (Dudley and DeVries, 1990); the associated aerodynamics, unfortunately, remain unknown.

Stability also appeared to be a problem during flight at the fastest speeds, with pronounced roll being particularly evident. The sensitivity to roll may result from the low angles of incidence at which the wings are operating and from the spanwise gradients in both wing twist and relative velocity. It is likely that the angle of incidence switches sign at some point along the wing on the upstroke. Different areas of the wing would then be fulfilling different roles: the proximal regions providing weight support, and the distal regions generating thrust. The angles of incidence in the middle of the wing will be close to zero and, therefore, very sensitive to slight changes in the relative velocity and wing orientation. The difficulty experienced by many moths in controlling steady flight at these speeds was also seen in the side-view image. Flight often consisted of alternating periods, of only two or three wingbeats each, in which the moth accelerated towards the feeder, before slipping backwards and slightly down to its original position.

Morphology and aerodynamics

The morphological data for *Manduca sexta* indicate that, whilst there is little variation within each sex, there are significant differences between males and females. The larger size of the females, in terms of both wing length and body mass, and their shorter bodies relative to wing length, support previous observations by R. D. Stevenson (unpublished data) concerning the gross morphological parameters. Much of the increased mass of the females is contained in their abdomens, which are swollen with eggs. This alters the mass distribution and results in a posterior shift of the centre of mass. The increased distance between the centre of mass and the wingbases has a detrimental effect on the responsiveness of the body in the pitching plane since larger moments are required to change the body angle (Ellington, 1984*b*). The marked discrepancy between the free body angles and the body angles observed during flight means that the pitching moments are likely to be substantial. As the females age, their abdomens will lighten as a result of oviposition, and their pitching performance should become closer to that of the males.

The wings of the females have a significantly higher aspect ratio than those of the males, indicating that they are narrower relative to their length. Despite their greater absolute length, the females have a lower wing area per unit body mass than the males, which is reflected in their higher wing loading and lower wing mass as a proportion of body mass. The difference in wing loading has implications for both the mechanics and cost of flight (Ellington, 1984*e*; Norberg, 1990; Spedding, 1992). The higher wing loading in females is not matched by the mean thickness of their wings, which was only 0.07 % of the wing length compared with 0.08 % in the males.

There was remarkably little variation in the radii for the moments of wing area. A comparison of the values for males and females indicated that wing shape is highly conserved between the two sexes, as it is between the two subfamilies of the Sphingidae (Casey and Stevenson, 1989). There were significant gender differences in the radii for virtual mass, but the magnitude of these differences was only approximately 0.5 % of wing length.

The derivation of non-dimensional morphological parameters allows meaningful comparison between different species which can provide clues as to the functional significance of these parameters. Ellington (1984*b*) gathered a data set from a number of sources which included representative species from the Coleoptera, Diptera, Hymenoptera, Neuroptera and Odonata, as well as the Lepidoptera (of which *Manduca sexta* was one). Individual groups which have been investigated in more detail are the Diptera (Dudley, 1987; Ennos, 1989) and the Papilionoidea and Hesperioidea (Betts and Wootton, 1988; Bunker, 1993). Whilst the small sample sizes for many of the species prevent a quantitative investigation of interspecific differences, a number of qualitative observations can be made concerning where the results for *Manduca sexta* fit into the spectrum of insect morphologies.

The wings of *Manduca sexta* are comparatively long relative to their body length and, in conjunction with a lower aspect ratio than any other group except for the butterflies, this results in a large wing area per unit body mass. This is shown by wing loadings (a mean of 7.8 N m^{-2} for males and 9.7 N m^{-2} for

females) which are markedly lower than those of hymenopterans (as high as 35.6 N m^{-2} in *Bombus terrestris* queens; Dudley and Ellington, 1990*b*), although higher than the range from approximately 2 to 4 N m^{-2} recorded for butterflies (Betts and Wootton, 1988; Bunker, 1993).

The non-dimensional radii of the moments of wing area and virtual mass for *Manduca sexta* and the other lepidopterans are smaller than those for other insect groups. This concentration of area close to the wingbase is largely a consequence of the coupling of a long, narrow forewing with a short, broad hindwing. This trend is more pronounced in *Manduca sexta* than in the hymenopterans, whose radii are approximately 10 % greater as a result (Ellington, 1984*b*). The hindwings in the Papilionoidea and Hesperioidea tend to be broader still than those of the hawkmoths, and this is reflected in even lower values for these radii (Betts and Wootton, 1988; Bunker, 1993). Similarly, the radii for the moments of wing mass are lower than average in the Lepidoptera, indicating that the mass distribution is also skewed towards the wingbase. For a given wing mass, lower radii have direct significance for the mechanics of flight because they reduce the corresponding moment about the wingbase, and thus the inertial costs of flight. This may help to offset the increased mass associated with the high relative thickness of the wings, a trait which is typical of 'advanced' wings with a few, thick veins (Ellington, 1984*b*). The concentration of wing area in the proximal half of the wing reduces the lift force generated during flapping flight, but it also reduces the profile power component.

The large distance between the wingbase and the centre of mass of the body in *Manduca sexta*, when compared with the dipteran and hymenopteran species, has a detrimental influence on the pitching manoeuvrability of the hawkmoths, as discussed above. This does not, however, appear to have any great consequences for *Manduca sexta*: they are less agile fliers than hoverflies, for example, but their flight is still sufficiently versatile to fulfil its roles in nutrition and reproduction.

Aerodynamic force coefficients

There have only been a limited number of studies of the aerodynamic characteristics of insect bodies and wings, and the flow around these structures is poorly understood. A comparison of the force coefficients for *Manduca sexta* with the results for other species does, however, raise a number of interesting observations about the performance of both the body and the wings.

The drag coefficient of an insect body at zero angle of attack is one measure of the extent of its streamlining. Recalculating this value for *Manduca sexta* based on frontal rather than planform area, to allow comparison with earlier studies, gives a drag coefficient between 0.25 and 0.3 which is relatively independent of Reynolds number. These values are substantially lower than the minimum coefficients recorded for all the other species: 1.1 for large flies and 2.3 for small flies (Hocking, 1953), 1.47 for locusts (Weis-Fogh, 1956), 1.16 for *Drosophila virilis* (Vogel, 1967), 0.63 for bumblebee workers (Dudley and Ellington, 1990*b*), 0.45 for the honeybee (Nachtigall and Hanauer-Thieser, 1992), and between 0.45 and 0.5 for dragonflies and damselflies (Wakeling and Ellington, 1997*a*). The data, therefore, confirm Brodsky and Ivanov's (1974, quoted in Brodsky, 1994) conclusion that the hawkmoth body plan is the most streamlined seen among insects.

The relationship between drag coefficient and Reynolds number is not clear. A decrease from 1.0 to 0.63 was seen in bumblebees as Re_b increased from 1000 to 4000 (Dudley and Ellington, 1990*b*), and in the honeybee from 1.36 to 0.45 as Re_b increased from 400 to 3970 (Nachtigall and Hanauer-Thieser, 1992). This will help to limit the rapid increase in parasite drag at fast forward speeds (Spedding, 1992). The decrease in drag coefficient for the honeybee was steepest at Reynolds numbers below 2000, which corresponds to the results obtained by Hertel (1963) for a range of body shapes. All of the *Manduca sexta* measurements were made at Reynolds numbers higher than this, which may explain the lack of variation in the drag coefficient.

The characteristics of the *Manduca sexta* body are unlikely to have been significantly affected by the absence of the legs and antennae. Nachtigall and Hanauer-Thieser (1992) found that the drag on honeybee bodies was unaffected by removal of the legs, although the slight change in frontal area was reflected in a slight increase in drag coefficient. If planform area is used, as it was here, then the legs have only a negligible effect. An upper limit to the additional drag due to the antennae was estimated by calculating the drag on cylinders of the same size aligned normal to the flow, using the expressions in Ellington (1991). At the highest speed recorded for each moth, the total drag on the antennae would be 1.5 and 1.8 % of body weight for moths F1 and F2, respectively, and 3.2 % for moth M1. The additional parasite power at these speeds would have added 3–4 % to the total aerodynamic power (Willmott, 1995).

The importance of the contribution of body lift to the vertical force balance has been a matter of some contention. Body lifts of up to one-third of body weight reported by Hocking (1953) have not been repeated for other species. At angles appropriate to fast forward flight, when body lift should be highest, the contribution from the body was less than 5 % in locusts (Jensen, 1956), a cockchafer (Nachtigall, 1964), some dipterans (Wood, 1970) and a honeybee (Nachtigall and Hanauer-Thieser, 1992), and 10 % or less in a noctuid moth (Chance, 1975) and a bumblebee (Dudley and Ellington, 1990*b*). Under the same conditions, the maximum body lift observed for *Manduca sexta* was also approximately 10 % of body weight, and it seems likely that this value is close to the upper limit for the contribution of body lift in most flying insects.

The steady-state performance of the hawkmoth wing, as measured by the maximum lift:drag ratio, is impressive for an insect. Very high values of more than 15 have recently been recorded for odonatan wings whose minimum drag coefficient was found at a non-zero, positive angle of attack (Wakeling and Ellington, 1997*a*). Amongst other species, however, the ratio of approximately 4 for *Manduca sexta* is second only to the value of 8 recorded for the locust hindwing (Jensen, 1956),

and the accuracy of the latter has been queried because the measured minimum drag coefficient is lower than theoretically possible (Ellington, 1984*d*). The results for *Manduca sexta*, the odonatans and the locust match the conclusions of Spedding (1992) and Brodsky (1994) that the highest lift:drag ratios are found at the high Reynolds numbers characteristic of large, fast-flying insects whose wings operate under flow conditions where inertial forces dominate. Maximum lift coefficient is relatively independent of Reynolds number, lying in the range from approximately 0.7 to 0.9 for most species studied, and the variation in the lift:drag ratio results from the friction drag component of profile drag scaling as $Re^{-0.5}$ (Blasius, 1908). The relative contribution of friction drag is highest at the low angles of attack where the maximum lift:drag ratios occur. The minimum value of the drag coefficient for *Manduca sexta* wings was 0.05, for example, compared with 0.25 and 0.13 for a bumblebee worker at Reynolds numbers of 460 and 1240, respectively (Dudley and Ellington, 1990*b*), and 0.54 and 0.29 for cambered *Drosophila virilis* wings at Reynolds numbers of 65 and 260, respectively (Vogel, 1967).

As the Reynolds number decreases, the maximum C_L:C_D ratio also decreases, but the wings display a very gentle stall. These characteristics can be seen in the polar diagrams for the mayfly *Ephemera vulgata* (C_L:C_D=3.3; Brodsky, 1970), the cranefly *Tipula oleracea* (C_L:C_D=2.4; Nachtigall, 1977) and the bumblebee *Bombus terrestris* (Dudley and Ellington, 1990*b*) whose C_L:C_D ratio was approximately 2.5 at Reynolds numbers from 460 to 1520. At even lower Reynolds numbers, the increasing importance of viscous effects reduces the lift:drag ratio further but leads to the virtual absence of stall, which was seen with the wings of *Drosophila virilis* at Reynolds numbers between 65 and 260 (Vogel, 1967).

The details of the airflow around insect wings under steady-state conditions are not well understood, but a number of structural features that influence aerodynamic performance have been identified, and some of these can be seen in the hawkmoth wing. The most widespread feature is the beneficial effect of wing camber in increasing lift coefficients at positive angles of attack. Vogel (1967) found that the polar diagram for flat *Drosophila virilis* wings was nearly symmetrical about the 0° angle-of-attack position, but that the addition of camber resulted in a positive shift in lift coefficients which was most pronounced for positive angles of attack. Similarly, the convex profile seen in locust forewings during late downstroke increased the lift:drag ratio of the wing (Jensen, 1956). The small, but consistent, positive camber inherent in the *Manduca sexta* wing structure probably contributed to the better performance of the wing at positive than at negative angles of attack, and it is likely to enhance lift production during the long downstroke of flapping flight when the wing profile is similar to that of the isolated wing couples in this study.

The same wing shape is, however, unlikely to be such an accurate model of the wings during the upstroke, and this may, in part, explain the asymmetry between the lift coefficients at positive and negative angles of attack. The wing twist and camber during the upstroke have not been as well quantified as those of the downstroke (Willmott and Ellington, 1997) but, qualitatively, the wing shape appears to be both more complicated and more variable during the former. In addition, the direction of camber (at least in the regions posterior to the rigid leading-edge spar) may be the reverse of that used here. The lift and drag coefficients measured at negative angles of attack in this study may, therefore, underestimate the true steady-state values for the hawkmoth wing couple configuration appropriate to upstroke periods when the wing is acting at negative angles of incidence. In terms of the aerodynamic analysis undertaken here, however, any discrepancies in these force coefficients would only have had a noticeable impact on the values for profile drag and profile power estimated from the observed angles of incidence.

An important role for leading-edge separation bubbles in shaping wing performance through the avoidance of abrupt stall and the enhancement of lift production has been proposed (Ellington, 1984*c*; Spedding, 1992). Leading-edge vorticity had a strong influence on the flow around the wings during *Manduca sexta* flapping flight at all speeds (Ellington *et al.* 1996; Willmott *et al.* 1997), and it may also explain the gradual stall seen in Fig. 2 and the marked difference in performance of the *Manduca sexta* wing between a Reynolds number of 1150 and the two higher values. This discrepancy has not been seen before for insect wings, but it may represent the increase in lift production which accompanies the formation of a strong leading-edge separation bubble at Re_c=3300 and Re_c=5560. The wing performance at negative angles of attack is similar for all three Reynolds numbers, and it mirrors the curve for positive angles at the lowest Reynolds number, suggesting that any separation bubbles are comparable under these flow conditions. Visualization of the flow around the wings is needed in order to confirm these hypotheses.

The possibility cannot be excluded from these data that the slight delay between the force measurements at Re_c=1150 and at Re_c=3300 and 5560 might have contributed to the differences in the force coefficients. A number of observations suggest, however, that the differences probably represent a genuine aerodynamic phenomenon. First, the *Manduca sexta* wing is a rigid structure, even when fresh, and there is little qualitative change in this over 24 h, or over much longer periods. Second, the discrepancy was only in the coefficients at positive angles of attack. At negative angles, the performance of the wings was similar at all speeds. Finally, the unusually low coefficients were obtained on the first day, with the later results being closer to the coefficients recorded for other species. The maximum lift coefficients at Re_c=3300 and Re_c=5560 were, for example, very similar to those obtained from the wing couple of a noctuid moth at 5 m s^{-1} (Lendle, 1981, cited in Nachtigall, 1989).

Directions for future studies

This study has identified the manner in which the mean lift coefficient varies with changes in wing kinematics. The requirement for unsteady aerodynamic mechanisms is clear, but their precise nature and contribution cannot be ascertained

from the mean coefficients model. Future models must incorporate new techniques which can accurately simulate both the flow around the wings and the instantaneous forces. Such models will allow full investigation of the impact of structures such as leading-edge vortices: the benefits of unsteady mechanisms in terms of lift production have often been cited, but there is also likely to be an associated cost through, for example, increased profile drag.

Symbols

AR	Aspect ratio
A_x, A_z	Summations used in calculating the horizontal and vertical components of lift, respectively.
B_x, B_z	Summations used in calculating the horizontal and vertical components of profile drag, respectively.
c	Wing chord
$\hat{c}$	Wing chord/mean chord
$\bar{c}$	Mean wing chord
C_D	Drag coefficient
$C_{D,pro}$	Profile drag coefficient
$\bar{C}_{D,pro}$	Mean profile drag coefficient
C_L	Lift coefficient
$\bar{C}_L$	Mean lift coefficient
D	Drag
D_{par}	Parasite drag
$\hat{D}_{par}$	Parasite drag/body weight
D_{pro}	Profile drag
F_x	Horizontal force required from the wings to overcome parasite drag
F_z	Vertical force required from the wings to complete the force balance
g	Gravitational acceleration
$\hat{h}$	Mean thickness of the wing/wing length
i	Wing strip number
I	Moment of inertia
J	Advance ratio ($V/\bar{U}_t$)
k	Reduced frequency parameter *or* correction factor for spatial and temporal variation in induced velocity
l	Characteristic length for calculating wing or body Reynolds numbers
$\hat{l}$	Distance from anterior tip of body to centre of mass/body length
$\hat{l}_1$	Distance from forewing base axis to centre of mass/body length
$\hat{l}_2$	Radius of gyration for the body/body length
L	Lift *or* body length
$\hat{L}$	Body length/wing length
L_{par}	Parasite lift: vertical force acting on the body
$\hat{L}_{par}$	Parasite lift/body weight
m	Body mass
$\hat{m}_a$	Mass of the abdomen/body mass
$\hat{m}_t$	Mass of the thorax/body mass
$\hat{m}_{tm}$	Mass of the thoracic muscle/body mass
$\hat{m}_w$	Wing mass/body mass
n	Wingbeat frequency
p_w	Wing loading
P^*	Body-mass- or muscle-mass-specific values of the power components
P_{acc}	Inertial power
P_{aero}	Total aerodynamic power
P_{ind}	Induced power
P_{par}	Parasite power
P_{pos}	Mean total positive mechanical power
P_{pro}	Profile power
r	Radial position along the wing
$\hat{r}$	Radial position along the wing/wing length
$\hat{r}_k(m)$	Radius of the kth moment of wing mass/wing length
$\hat{r}_k(S)$	Radius of the kth moment of wing area/wing length
$\hat{r}_k(v)$	Radius of the kth moment of wing virtual mass/wing length
R	Wing length
Re	Reynolds number
Re_b	Reynolds number for the body, based on body length
Re_c	Reynolds number for the wings, based on mean chord
S	Wing area
t	Time
U	Flapping velocity
U_n	Normal to the relative velocity
U_r	Relative velocity
$U_{r,b}$	Relative velocity of the body
U_t	Flapping velocity at the wingtip
$\bar{U}_t$	Mean flapping velocity at the wingtip
$\hat{v}$	Non-dimensional virtual mass of a wing pair (see Ellington, 1984*b*)
V	Flight velocity
w_0	Induced velocity at the actuator disc
$w_{0,RF}$	Rankine–Froude estimate of induced velocity at the actuator disc
α	Angle of attack
α_r	Angle of incidence
α_r'	Effective angle of incidence
α_{sp}	Angle of rotation relative to the stroke plane
θ	Angle of elevation of the wing with respect to the stroke plane
υ	Kinematic viscosity of air
ρ	Mass density of air
ρ_w	Mass density of the wings
ϕ	Sweep angle of the wing in the stroke plane
Φ	Stroke amplitude
χ	Body angle
$\chi_{r,b}$	Angle of incidence of the body
χ_0	Free body angle
ω	Radian frequency
Subscripts:	
ai	Using profile drag coefficients estimated from the angles of incidence

d	For the downstroke
s	For a sinusoidal approximation to the wingbeat
u	For the upstroke
x, z	Component in the *x* (horizontal) or *z* (vertical) direction.

We are very grateful to Dr J. M. Wakeling, Dr S. Sunada and Dr R. D. Stevenson for their help in many ways during the course of this study, and to Mr S. Ellis for manufacturing parts for the force transducer. This work was supported by grants from the BBSRC (A.P.W.), the SERC and the Hasselblad Foundation (C.P.E.).

References

ALDRIDGE, H. D. J. N. (1986). Kinematics and aerodynamics of the greater horseshoe bat, *Rhinolophus ferrumequinum*, in horizontal flight at various flight speeds. *J. exp. Biol.* **126**, 479–497.

BETTS, C. R. AND WOOTTON, R. J. (1988). Wing shape and flight behaviour in butterflies (Lepidoptera: Papilionoidea and Hesperioidea): a preliminary analysis. *J. exp. Biol.* **138**, 271–288.

BLASIUS, H. (1908). Grenzschichten in Flüssigkeiten mit kleiner Reibung. *Z. Math. Phys.* **56**, 1–37.

BRODSKY, A. K. (1970). On the role of wing pleating in insects. *Zh. evol. biochem. physiol.* **6**, 470–471.

BRODSKY, A. K. (1994). *The Evolution of Insect Flight*. Oxford: Oxford University Press.

BRODSKY, A. K. AND IVANOV, V. D. (1974). Aerodynamic peculiarities of the flight of insects. II. Smoke spectra. *Vestnik Leningr. Univ. (Biology)* **3**, 16–21.

BRODSKY, A. K. AND IVANOV, V. D. (1984). The role of vortices in insect flight. *Zool. Zhurn.* **63**, 197–208.

BUNKER, S. J. (1993). Form, flight pattern and performance in butterflies (Lepidoptera: Papilionoidea and Hesperioidea). PhD thesis, University of Exeter.

CASEY, T. M. (1976). Flight energetics of sphinx moths: power input during hovering flight. *J. exp. Biol.* **64**, 529–543.

CASEY, T. M. (1981). A comparison of mechanical and energetic estimates of flight cost for hovering sphinx moths. *J. exp. Biol.* **91**, 117–129.

CASEY, T. M. AND STEVENSON, R. D. (1989). A comparative analysis of wing morphology and frequency in moths of the family Sphingidae. *Am. Soc. Zool.* **29**, 82A.

CHANCE, M. A. C. (1975). Air flow and the flight of a noctuid moth. In *Swimming and Flying in Nature*, vol. 2 (ed. T. Y. Wu., C. J. Brokaw and C. Brennen), pp. 829–843. New York: Plenum Press.

COOPER, A. J. (1993). Limitations of bumblebee flight performance. PhD thesis, University of Cambridge.

DICKINSON, M. H. AND LIGHTON, J. R. B. (1995). Muscle efficiency and elastic storage in the flight motor of *Drosophila*. *Science* **268**, 87–90.

DUDLEY, R. (1987). The mechanics of forward flight in insects. PhD thesis, University of Cambridge.

DUDLEY, R. (1990). Biomechanics of flight in neotropical butterflies: morphometrics and kinematics. *J. exp. Biol.* **150**, 37–53.

DUDLEY, R. (1995). Extraordinary flight performance of orchid bees (Apidae: Euglossini) hovering in heliox (80 % He/20 % O_2). *J. exp. Biol.* **198**, 1065–1070.

DUDLEY, R. AND DEVRIES, P. J. (1990). Flight physiology of migrating *Urania fulgens* (Uraniidae) moths: kinematics and aerodynamics of natural free flight. *J. comp. Physiol.* A **167**, 145–154.

DUDLEY, R. AND ELLINGTON, C. P. (1990*a*). Mechanics of forward flight in bumblebees. I. Kinematics and morphology. *J. exp. Biol.* **148**, 19–52.

DUDLEY, R. AND ELLINGTON, C. P. (1990*b*). Mechanics of forward flight in bumblebees. II. Quasi-steady lift and power requirements. *J. exp. Biol.* **148**, 53–88.

ELLINGTON, C. P. (1980). Vortices and hovering flight. In *Instationäre Effekte an schwingenden Tierflügeln* (ed. W. Nachtigall), pp. 64–101. Wiesbaden: Franz Steiner.

ELLINGTON, C. P. (1984*a*). The aerodynamics of hovering insect flight. I. The quasi-steady analysis. *Phil. Trans. R. Soc. Lond. B* **305**, 1–15.

ELLINGTON, C. P. (1984*b*). The aerodynamics of hovering insect flight. II. Morphological parameters. *Phil. Trans. R. Soc. Lond. B* **305**, 17–40.

ELLINGTON, C. P. (1984*c*). The aerodynamics of hovering insect flight. IV. Aerodynamic mechanisms. *Phil. Trans. R. Soc. Lond. B* **305**, 79–113.

ELLINGTON, C. P. (1984*d*). The aerodynamics of hovering insect flight. V. A vortex theory. *Phil. Trans. R. Soc. Lond. B* **305**, 115–144.

ELLINGTON, C. P. (1984*e*). The aerodynamics of hovering insect flight. VI. Lift and power requirements. *Phil. Trans. R. Soc. Lond. B* **305**, 145–181.

ELLINGTON, C. P. (1991). Aerodynamics and the origin of insect flight. *Adv. Insect Physiol.* **23**, 171–210.

ELLINGTON, C. P. (1995). Unsteady aerodynamics of insect flight. In *Biological Fluid Dynamics* (ed. C. P. Ellington and T. J. Pedley). *Symp. Soc. exp. Biol.* **49**, 109–129. Cambridge: Company of Biologists.

ELLINGTON, C. P., VAN DEN BERG, C., WILLMOTT, A. P. AND THOMAS, A. L. R. (1996). Leading-edge vortices in insect flight. *Nature* **384**, 626–630.

ENNOS, A. R. (1989). The kinematics and aerodynamics of the free flight of some Diptera. *J. exp. Biol.* **142**, 49–85.

HERTEL, H. (1963). *Biologie und Technik.* Mainz: Krausskopf.

HOCKING, B. (1953). The instrinsic range and speed of flight of insects. *Trans. R. ent. Soc. Lond.* **104**, 223–345.

JENSEN, M. (1956). Biology and physics of locust flight. III. The aerodynamics of locust flight. *Phil. Trans. R. Soc. Lond. B* **239**, 511–552.

LENDLE, K. (1981). Untersuchungen zur Erzeugung stationärer Auftriebs-und Widerstandskräfte an Insektenflügeln mittels einer umschaltbaren aerodynamischen Einkomponentenwaage. Staatsexamensarbeit, Universität des Saarlandes, Saarbrücken.

LIU, H., WASSERSUG, R. J. AND KAWACHI, K. (1996). A computational fluid dynamics study of tadpole swimming. *J. exp. Biol.* **199**, 1245–1260.

NACHTIGALL, W. (1964). Zur Aerodynamik des Coleopteren flugs: Wirken die Elytren als Tragflügel? *Verh. dt. zool. Ges.* **52**, 319–326.

NACHTIGALL, W. (1966). Die Kinematik der Schlagflügelbewegungen von Dipteren. Methodische und Analytische Grundlagen zur Biophysik des Insektenflugs. *Z. vergl. Physiol.* **52**, 155–211.

NACHTIGALL, W. (1977). Die aerodynamische Polare des Tipula-Flügels und eine Einrichtung zur halbautomatischen Polarenaufnahme. In *The Physiology of Movement; Biomechanics* (ed. W. Nachtigall), pp. 347–352. Stuttgart: Fischer.

NACHTIGALL, W. (1989). Mechanics and aerodynamics of flight. In *Insect Flight* (ed. G. J. Goldsworthy and C. H. Wheeler), pp. 1–29. Boca Raton, FL: CRC Press.

NACHTIGALL, W. AND HANAUER-THIESER, U. (1992). Flight of the

honeybee. V. Drag and lift coefficients of the bee's body; implications for flight dynamics. *J. comp. Physiol.* B **162**, 267–277.

NORBERG, U. M. (1976). Aerodynamics, kinematics and energetics of horizontal flight in the long-eared bat *Plecotus auritus*. *J. exp. Biol.* **65**, 179–212.

NORBERG, U. M. (1985). Flying, gliding and soaring. In *Functional Vertebrate Morphology* (ed. M. Hildebrand, D. M. Bramble, K. F. Liem and D. B. Wake), pp. 129–158. Cambridge, MA: Harvard University Press.

NORBERG, U. M. (1990). *Vertebrate Flight.* Berlin: Springer-Verlag.

OSBORNE, M. F. M. (1951). Aerodynamics of flapping flight with application to insects. *J. exp. Biol.* **28**, 221–245.

PENNYCUICK, C. J. (1968). Power requirements for horizontal flight in the pigeon *Columba livia*. *J. exp. Biol*. **49**, 527–555.

PENNYCUICK, C. J. (1975). Mechanics of flight. In *Avian Biology*, vol. 5 (ed. D. S. Farner and J. R. King), pp. 1–75. London: Academic Press.

RAYNER, J. M. V. (1979). A new approach to animal flight mechanics. *J. exp. Biol*. **80**, 17–54.

RAYNER, J. M. V. (1986). Vertebrate flapping flight mechanics and aerodynamics and the evolution of flight in bats. In *Bat Flight – Fledermausflug. BIONA Report 5* (ed. W. Nachtigall), pp. 27–74. Stuttgart: Fischer.

SMITH, M. J. C. (1996). Simulating moth wing aerodynamics: towards the development of flapping-wing technology. *AIAA J.* **34**, 1348–1355.

SMITH, M. J. C., WILKIN, P. J. AND WILLIAMS, M. H. (1996). The advantages of an unsteady panel method in modelling the aerodynamic forces on rigid flapping wings. *J. exp. Biol.* **199**, 1073–1083.

SPEDDING, G. R. (1987). The wake of a kestrel (*Falco tinnunculus*) in flapping flight. *J. exp. Biol.* **127**, 59–78.

SPEDDING, G. R. (1992). The aerodynamics of flight. In *Mechanics of Animal Locomotion* (ed. R. McN. Alexander). *Adv. comp. env. Physiol*. **11**, 51–111. Berlin: Springer-Verlag.

SPEDDING, G. R. AND DELAURIER, J. D. (1996). Animal and ornithopter flight. In *Handbook of Fluid Dynamics and Fluid Machinery. Vol. III: Applications of Fluid Dynamics* (ed. J. A. Schetz and A. E. Fuhs), pp. 1951–1967. New York: John Wiley & Sons.

SRYGLEY, R. B. AND DUDLEY, R. (1993). Correlations of the position of center of body mass with butterfly escape tactics. *J. exp. Biol.* **174**, 155–166.

STEPNIEWSKI, W. Z. AND KEYS, C. N. (1984). *Rotary-Wing Aerodynamics*. New York: Dover.

STEVENSON, R. D., CORBO, K., BACA, L. B. AND QUANG, D. LE. (1995). Cage size and flight speed of the tobacco hawkmoth *Manduca sexta*. *J. exp. Biol.* **198**, 1665–1672.

STEVENSON, R. D. AND JOSEPHSON, R. K. (1990). Effects of operating frequency and temperature on mechanical power output from moth flight muscle. *J. exp. Biol.* **149**, 61–78.

SUNADA, S., KAWACHI, K., WATANABE, I. AND AZUMA, A. (1993). Performance of a butterfly in take-off flight. *J. exp. Biol.* **183**, 249–277.

VISBAL, M. R. (1986). Evaluation of an implicit Navier–Stokes solver for some unsteady separated flows. *AIAA* Paper no. 86-1053.

VOGEL, S. (1967). Flight in *Drosophila.* III. Aerodynamic characteristics of fly wings and wing models. *J. exp. Biol.* **46**, 431–443.

WAKELING, J. M. AND ELLINGTON, C. P. (1997*a*). Dragonfly flight. I. Gliding flight and steady-state aerodynamic forces. *J. exp. Biol.* **200**, 543–556.

WAKELING, J. M. AND ELLINGTON, C. P. (1997*b*). Dragonfly flight. III. Lift and power requirements. *J. exp. Biol.* **200**, 583–600.

WEIS-FOGH, T. (1956). Biology and physics of locust flight. II. Flight performance of the Desert Locust (*Schistocerca gregaria*). *Phil. Trans. R. Soc. Lond. B* **239**, 459–510.

WEIS-FOGH, T. (1972). Energetics of hovering flight in hummingbirds and in *Drosophila*. *J. exp. Biol.* **56**, 79–104.

WEIS-FOGH, T. (1973). Quick estimates of flight fitness in hovering animals, including novel mechanisms for lift production. *J. exp. Biol.* **59**, 169–230.

WILKIN, P. J. AND WILLIAMS, M. H. (1993). Comparison of the aerodynamic forces on a flying sphingid moth with those predicted by quasi-steady theory. *Physiol. Zool.* **66**, 1015–1044.

WILLMOTT, A. P. (1995). The mechanics of hawkmoth flight. PhD thesis, University of Cambridge.

WILLMOTT, A. P. AND ELLINGTON, C. P. (1997). The mechanics of flight in the hawkmoth *Manduca sexta*. I. Kinematics of hovering and forward flight. *J. exp. Biol.* **200**, 2705–2722.

WILLMOTT, A. P., ELLINGTON, C. P. AND THOMAS, A. L. R. (1997). Flow visualization and unsteady aerodynamics in the flight of the hawkmoth *Manduca sexta*. *Phil. Trans. R. Soc. Lond. B* **352**, 303–316.

WOOD, J. (1970). A study of the instantaneous air velocities in a plane behind the wings of certain Diptera flying in a wind tunnel. *J. exp. Biol.* **52**, 17–25.